

The new Z' boson of the Bestest Little Higgs Model as a portal to signatures of Higgs bosons h_0 and H_0 at the future muon collider

J. M. Martínez-Martínez^{*,1} A. Gutiérrez-Rodríguez^{†,1}

E. Cruz-Albaro^{‡,1} and M. A. Hernández-Ruíz^{§2}

¹*Facultad de Física, Universidad Autónoma de Zacatecas*

Apartado Postal C-580, 98060 Zacatecas, México.

²*Unidad Académica de Ciencias Químicas, Universidad Autónoma de Zacatecas*

Apartado Postal C-585, 98060 Zacatecas, México.

(Dated: June 4, 2024)

Abstract

We study the new Z' boson as a portal for the production of Higgs bosons h_0 and H_0 predicted by the Bestest Little Higgs Model through the Higgs-strahlung processes $\mu^+\mu^- \rightarrow (Z, Z') \rightarrow Zh_0, ZH_0$. We focus on the resonance and non-resonance effects of the Zh_0, ZH_0 signals. In our analysis, we consider the center-of-mass energies of $\sqrt{s} = 3, 4, 5, 6, 7, 10, 30$ TeV and integrated luminosities of $\mathcal{L} = 2, 4, 6, 10, 30$ ab^{-1} projected for a future muon collider. The possibility of performing precision measurements for the Higgs bosons h_0 and H_0 is very promising at the future muon collider. Furthermore, our results may be helpful to the High Energy Physics community. Complementarily, we generate and provide the Feynman rules necessary for studying the processes $\mu^+\mu^- \rightarrow (Z, Z') \rightarrow Zh_0, ZH_0$.

PACS numbers: 12.60.-i, 12.15.Mm, 13.66.Fg

Keywords: Models beyond the standard model, neutral currents, gauge, and Higgs boson production in $\mu^+\mu^-$ interactions.

* jose.martinez@fisica.uaz.edu.mx

† alexgu@fisica.uaz.edu.mx

‡ elicruzalbaro88@gmail.com

§ mahernan@uaz.edu.mx

I. INTRODUCTION

Since the confirmation of the existence of the Higgs boson by the ATLAS [1] and the CMS [2] Collaborations at the Large Hadron Collider (LHC), the scientific community has undertaken the task of confirming that its properties match those of the scalar boson predicted by the Standard Model (SM) [3–7]. Despite the great predictive power of the SM, there are unsolved problems, such as the hierarchy problem. Namely, quantum corrections render the Higgs potential fine-tuned. These quantum corrections come from three different sectors of the SM: the gauge sector, the fermion sector, and the Higgs sector. To have a theory that is not fine-tuned, new physics is needed in each of these three sectors to cancel quantum corrections to the Higgs potential.

Various extensions of the SM have been proposed to solve the hierarchy problem. Some of the proposed extensions are the Little Higgs Models (LHM) [8–12] that employ a mechanism named collective symmetry breaking. Its main idea is to represent the SM Higgs boson as a pseudo-Nambu-Goldstone boson of an approximate global symmetry spontaneously broken at a scale in the TeV range. In these models, the collective symmetry-breaking mechanisms are implemented in the gauge, fermion, and Higgs sectors, which predict new particles within the mass range of a few TeV. These new particles play the role of partners of the top quark, of the gauge bosons, and the Higgs boson, the effect of which is to generate radiative corrections for the mass of the Higgs boson and, thus cancel the divergent corrections induced by SM particles. The LHM [8–12], on the other hand, already have strong constraints from electroweak precision measurements in the gauge sector [13–15], but also predict heavy top partners that are much heavier than the mass of the new gauge bosons, which leads to significant fine-tuning in the Higgs potential [13, 16].

A proposed model called the Bestest Little Higgs Model (BLHM) [13, 17, 18] overcomes the difficulties presented by LHM, which is achieved by incorporating two independent symmetry-breaking scales, f and F with $F > f$. In consequence, a disassociation in the masses of the fermion (T , B , T_5 , T_6 , $T^{2/3}$, $T^{5/3}$) and boson gauge (Z' , W'^{\pm}) partners is generated. In this way, the new quarks obtain masses proportional only to the f energy scale, while the new gauge bosons acquire masses proportional to the combination of the f and F scales. Since the new quarks are now lighter than the new gauge bosons, fine-tuning in the top sector and electroweak precision constraints in the gauge sector are avoided. On

the other hand, the scalar sector of the BLHM has a rich phenomenology generating the charged and neutral physical scalar fields: $h_0, H_0, A_0, \phi^0, \eta^0, H^\pm, \phi^\pm$ and η^\pm . The h_0 state is assumed to be light (≈ 125 GeV), similar to the Higgs boson of the SM, while the rest of the scalars can vary their masses.

In this paper, we explore the phenomenology of the production of the Higgs bosons h_0 and H_0 of the BLHM in muon collisions. Specifically, we will present a comprehensive analysis of the production mechanism $\mu^+\mu^- \rightarrow (Z, Z') \rightarrow Zh_0$ and $\mu^+\mu^- \rightarrow (Z, Z') \rightarrow ZH_0$ and its sensitivity including both the resonant and the non-resonant effects at future high-energy and high-luminosity muon collider. Our search of the Higgs bosons is implemented in the environment of a future muon collider [19, 20]. It is worth mentioning that a lepton collider is necessary to complement the LHC and study physics Beyond the Standard Model (BSM). Furthermore, a future muon collider offers certain advantages over a hadron collider as it could provide a potential solution to the issues regarding energy, luminosity, background cleanliness, and the limited sensitivity of current and other future colliders. These features make the muon collider an ideal collider for the search for new particles, as the first evidence of new physics is expected to arise in the TeV energy range. A high-energy, high-luminosity collider such as the muon collider will allow High Energy Physics to be explored at energy frontiers beyond the reach of existing and proposed colliders.

The outline of this paper is as follows: A review of the BLHM is presented in Section II. Section III presents the decay widths of the Z' boson at the BLHM. In Section IV, we find the scattering amplitudes and cross-sections of the processes $\mu^+\mu^- \rightarrow (Z, Z') \rightarrow Zh_0, ZH_0$. Section V is devoted to our numerical results. Finally, in Section VI, we present our conclusions. The Feynman rules involved in our calculations are provided in Appendix A.

II. A REVIEW OF THE BLHM

The BLHM [13, 17, 18, 21–27] is based on two independent non-linear sigma models. With the first field Σ , the global $SO(6)_A \times SO(6)_B$ symmetry is broken to the diagonal group $SO(6)_V$ at the energy scale f , while with the second field Δ , the global $SU(2)_C \times SU(2)_D$ symmetry is broken to the diagonal subgroup $SU(2)$ to the F scale when $F > f$. In the first stage are generated 15 pseudo-Nambu-Goldstone bosons that are parameterized as

$$\Sigma = e^{i\Pi/f} e^{2i\Pi_h/f} e^{i\Pi/f}, \quad (1)$$

where Π and Π_h are complex and antisymmetric matrices given by [13]

$$\Pi = \begin{pmatrix} i(\phi_a T_L^a + \eta_a T_R^a)_{4 \times 4} & 0 & 0 \\ 0 & 0 & i\sigma/\sqrt{2} \\ 0 & -i\sigma/\sqrt{2} & 0 \end{pmatrix}, \quad \Pi_h = \frac{i}{\sqrt{2}} \begin{pmatrix} 0_{4 \times 4} & h_1 & h_2 \\ -h_1^T & 0 & 0 \\ -h_2^T & 0 & 0 \end{pmatrix}. \quad (2)$$

In Eq. (2), ϕ_a and η_a ($a = 1, 2, 3$) are real triplets, h_1 and h_2 are $\mathbf{4}$'s of $SO(4)$, and σ a real singlet. For Higgs fields, their explicit representation is $h_i^T = (h_{i1}, h_{i2}, h_{i3}, h_{i4})$ (see Eqs. (16)-(23)), while $T_{L,R}^a$ denote the generators of the group $SO(6)$ which are provided in Refs. [13, 28]. Regarding the second stage of symmetry breaking, the pseudo-Nambu-Goldstone bosons of the field Δ are parameterized as follows

$$\Delta = F e^{2i\Pi_d/F}, \quad \Pi_d = \chi_a \frac{\tau_a}{2} \quad (a = 1, 2, 3), \quad (3)$$

χ_a represents the Nambu-Goldstone fields and the τ_a correspond to the Pauli matrices [13]. These latter are the generators of the $SU(2)$ group.

A. The scalar sector

To generate a viable Higgs quartic coupling in the BLHM, we must explicitly break some of the symmetries under which Higgs fields transform non-linearly. For this purpose, two operators are required, each of which explicitly breaks some of the global symmetries, but neither by itself would allow the Higgs to obtain a potential:

$$P_5 = \text{diag}(0, 0, 0, 0, 1, 0), \quad P_6 = \text{diag}(0, 0, 0, 0, 0, 1). \quad (4)$$

In this way, the quartic potential is written as

$$\begin{aligned} V_q &= \frac{1}{4} \lambda_{65} f^4 \text{Tr}(P_6 \Sigma P_5 \Sigma^T) + \frac{1}{4} \lambda_{56} f^4 \text{Tr}(P_5 \Sigma P_6 \Sigma^T) \\ &= \frac{1}{4} \lambda_{65} f^4 (\Sigma_{65})^2 + \frac{1}{4} \lambda_{56} f^4 (\Sigma_{56})^2, \end{aligned} \quad (5)$$

where λ_{65} and λ_{56} are coefficients that must be non-zero to achieve collective symmetry breaking and generate a successful Higgs quartic coupling. From Eq. (5), the first term breaks $SO(6)_A \times SO(6)_B \rightarrow SO(5)_{A6} \times SO(5)_{B5}$, the $SO(5)_{A6}$ transformation protects h_1 from getting a potential while $SO(5)_{B5}$ does the same for h_2 . Similarly, the second term in Eq. (5) explicitly breaks $SO(6)_A \times SO(6)_B \rightarrow SO(5)_{A5} \times SO(5)_{B6}$. This symmetry allows the singlet σ to get a potential while the other fields are protected. At this stage, if Eq. (1) is expanded as a power series in $1/f$ and substituted into Eq. (5), the following is obtained

$$V_q = \frac{\lambda_{65}}{2} \left(f\sigma - \frac{1}{\sqrt{2}} h_1^T h_2 + \dots \right)^2 + \frac{\lambda_{56}}{2} \left(f\sigma + \frac{1}{\sqrt{2}} h_1^T h_2 + \dots \right)^2. \quad (6)$$

In this expression, a mass term is generated for σ of the form $m_\sigma^2 = (\lambda_{65} + \lambda_{56})f^2$. No mass terms have been generated for the Higgs fields.

While each of the terms in Eq. (6) seems to generate a Higgs quartic coupling, this quartic coupling can be eliminated by a redefinition of the σ field as $\sigma \rightarrow \pm \frac{h_1^T h_2}{\sqrt{2}f}$, where the upper and lower signs of the transformation correspond to the first and second operators in the mentioned equation. Collectively, however, the two terms of Eq. (6) yield a tree-level Higgs quartic coupling, which occurs after the scalar σ is integrated out [13, 28, 29]. Therefore,

$$V_q = \frac{\lambda_{56}\lambda_{65}}{\lambda_{56} + \lambda_{65}} (h_1^T h_2)^2 = \frac{1}{2}\lambda_0 (h_1^T h_2)^2. \quad (7)$$

Eq. (7) has the desired form of a collective quartic potential [13, 28] and reaffirms that both terms of Eq. (6) are indeed necessary to generate a Higgs quartic coupling.

In the absence of gauge interactions, not all scalars obtain mass. Therefore, the following potential is added to generate them.

$$V_s = -\frac{f^2}{4} m_4^2 \text{Tr} \left(\Delta^\dagger M_{26} \Sigma M_{26}^\dagger + \Delta M_{26} \Sigma^\dagger M_{26}^\dagger \right) - \frac{f^2}{4} (m_5^2 \Sigma_{55} + m_6^2 \Sigma_{66}), \quad (8)$$

where m_4 , m_5 and m_6 are mass terms, and Σ_{55} and Σ_{66} represent the elements of the matrix Σ given in Eq. (1). On the other hand, M_{26} is a 2×6 matrix which contracts the $SU(2)$ indices of Δ with the $SO(6)$ indices of Σ :

$$M_{26} = \frac{1}{\sqrt{2}} \begin{pmatrix} 0 & 0 & 1 & i & 0 & 0 \\ 1 & -i & 0 & 0 & 0 & 0 \end{pmatrix}. \quad (9)$$

Expanding the operator Δ (see Eq. (3)) as a power series in $1/F$ and substituting in Eq. (8), we obtain

$$V_s = \frac{1}{2} (m_\phi^2 \phi_a^2 + m_\eta^2 \eta_a^2 + m_1^2 h_1^T h_1 + m_2^2 h_2^T h_2), \quad (10)$$

with

$$m_1^2 = \frac{1}{2}(m_4^2 + m_5^2), \quad (11)$$

$$m_2^2 = \frac{1}{2}(m_4^2 + m_6^2). \quad (12)$$

It is evident from Eq. (10) that the fields h_1 , h_2 , ϕ_a and η_a get their masses.

To destabilise the origin and trigger electroweak symmetry breaking, the following potential is also introduced

$$V_{B_\mu} = m_{56}^2 f^2 \Sigma_{56} + m_{65}^2 f^2 \Sigma_{65}, \quad (13)$$

where Σ_{56} and Σ_{65} denote the elements of the matrix Σ together with their mass parameters m_{56} and m_{65} , respectively. Finally, we have the full scalar potential of the BLHM,

$$V = V_q + V_s + V_{B_\mu}. \quad (14)$$

From this full potential, the potential for the Higgs doublet fields is obtained. For this task, one minimizes the potential of Eq. (14) concerning the scalar σ and substitutes the resulting solution for σ back into Eq. (14). This results in the following Higgs potential [13, 17, 30]

$$V_{Higgs} = \frac{1}{2} m_1^2 h_1^T h_1 + \frac{1}{2} m_2^2 h_2^T h_2 - B_\mu h_1^T h_2 + \frac{\lambda_0}{2} (h_1^T h_2)^2, \quad (15)$$

where the components of the Higgs doublets (h_1, h_2) , B_μ and λ_0 are explicitly expressed as

$$h_{11} = \cos \alpha h_0 - \sin \alpha H_0 + v \sin \beta, \quad (16)$$

$$h_{21} = \sin \alpha h_0 + \cos \alpha H_0 + v \cos \beta, \quad (17)$$

$$h_{12} = \cos \beta A_0, \quad (18)$$

$$h_{22} = \sin \beta A_0, \quad (19)$$

$$h_{13} = \frac{1}{\sqrt{2}} (\cos \beta (H^- + H^+)), \quad (20)$$

$$h_{14} = \frac{i}{\sqrt{2}} (\cos \beta (H^- - H^+)), \quad (21)$$

$$h_{23} = \frac{1}{\sqrt{2}} (\sin \beta (H^- + H^+)), \quad (22)$$

$$h_{24} = \frac{i}{\sqrt{2}} (\sin \beta (H^- - H^+)), \quad (23)$$

$$B_\mu = 2 \frac{\lambda_{56} m_{65}^2 + \lambda_{65} m_{56}^2}{\lambda_{56} + \lambda_{65}}, \quad (24)$$

$$\lambda_0 = 2 \frac{\lambda_{56} \lambda_{65}}{\lambda_{56} + \lambda_{65}}. \quad (25)$$

For the Higgs potential to reach a minimum, one must have $m_1 m_2 > 0$, while electroweak symmetry breaking requires that $B_\mu > m_1 m_2$.

Electroweak symmetry breaking in the BLHM is implemented when the Higgs doublets acquire their vacuum expectation values (VEVs), $\langle h_1 \rangle^T = (v_1, 0, 0, 0)$ and $\langle h_2 \rangle^T = (v_2, 0, 0, 0)$. These VEVs minimize the Higgs potential of Eq. (15), thus generating the following relations

$$v_1^2 = \frac{1}{\lambda_0} \frac{m_2}{m_1} (B_\mu - m_1 m_2), \quad (26)$$

$$v_2^2 = \frac{1}{\lambda_0} \frac{m_1}{m_2} (B_\mu - m_1 m_2). \quad (27)$$

The VEVs can be expressed in terms of the parameters v (the SM VEV) and $\tan \beta$ as follows

$$v^2 \equiv v_1^2 + v_2^2 = \frac{1}{\lambda_0} \left(\frac{m_1^2 + m_2^2}{m_1 m_2} \right) (B_\mu - m_1 m_2) \simeq (246 \text{ GeV})^2, \quad (28)$$

$$\tan \beta = \frac{v_1}{v_2} = \frac{m_2}{m_1}. \quad (29)$$

After electroweak symmetry breaking, the scalar sector of the BLHM generates several massive states: two physical scalar fields (H^\pm) and three neutral physical scalar fields (h_0 ,

H_0, A_0). The lightest state, h_0 , is identified as the Higgs boson of the SM. On the other hand, the four parameters in the Higgs potential m_1, m_2, B_μ , and λ_0 can be replaced by another more phenomenologically accessible set [17]. That is, the masses of the states h_0 and A_0 , the angle β and the VEV v :

$$1 < \tan \beta < \sqrt{\frac{2 + 2\sqrt{\left(1 - \frac{m_{h_0}^2}{m_{A_0}^2}\right)\left(1 - \frac{m_{h_0}^2}{4\pi v^2}\right)}}{\frac{m_{h_0}^2}{m_{A_0}^2}\left(1 + \frac{m_{A_0}^2 - m_{h_0}^2}{4\pi v^2}\right)}} - 1, \quad (30)$$

$$B_\mu = \frac{1}{2}(\lambda_0 v^2 + m_{A_0}^2) \sin 2\beta, \quad (31)$$

$$\lambda_0 = \frac{m_{h_0}^2}{v^2} \left(\frac{m_{h_0}^2 - m_{A_0}^2}{m_{h_0}^2 - m_{A_0}^2 \sin^2 2\beta} \right), \quad (32)$$

$$\tan \alpha = \frac{B_\mu \cot 2\beta + \sqrt{(B_\mu^2/\sin^2 2\beta) - 2\lambda_0 B_\mu v^2 \sin 2\beta + \lambda_0^2 v^4 \sin^2 2\beta}}{B_\mu - \lambda_0 v^2 \sin 2\beta}, \quad (33)$$

$$m_{H^\pm}^2 = m_{A_0}^2 = m_1^2 + m_2^2, \quad (34)$$

$$m_{H_0}^2 = \frac{B_\mu}{\sin 2\beta} + \sqrt{\frac{B_\mu^2}{\sin^2 2\beta} - 2\lambda_0 B_\mu v^2 \sin 2\beta + \lambda_0^2 v^4 \sin^2 2\beta}, \quad (35)$$

$$m_\sigma^2 = (\lambda_{56} + \lambda_{65})f^2 = 2\lambda_0 f^2 K_\sigma \quad \text{with} \quad 1 < K_\sigma < \frac{16\pi^2}{\lambda_0(8\pi - \lambda_0)}. \quad (36)$$

The variables λ_{56} and λ_{65} in Eq. (36) represent the coefficients of the quartic potential [13], both variables take values different from zero to achieve the collective breaking of the symmetry and generate a quartic coupling of the Higgs boson [13, 17].

B. The gauge sector

The kinetic terms of the gauge fields in the BLHM are given as follows:

$$\mathcal{L} = \frac{f^2}{8} \text{Tr}(D_\mu \Sigma^\dagger D^\mu \Sigma) + \frac{F^2}{4} \text{Tr}(D_\mu \Delta^\dagger D^\mu \Delta), \quad (37)$$

where the covariant derivatives are given by

$$D_\mu \Sigma = \partial_\mu \Sigma + ig_A A_{1\mu}^a T_L^a \Sigma - ig_B \Sigma A_{2\mu}^a T_L^a + ig_Y B_\mu^3 (T_R^3 \Sigma - \Sigma T_R^3), \quad (38)$$

$$D_\mu \Delta = \partial_\mu \Delta + ig_A A_{1\mu}^a \frac{\tau^a}{2} \Delta - ig_B \Delta A_{2\mu}^a \frac{\tau^a}{2}. \quad (39)$$

In these expressions, T_L^a are the generators of the group $SO(6)_A$ corresponding to the subgroup $SU(2)_{LA}$, while T_R^3 represents the third component of the $SO(6)_B$ generators corresponding to the $SU(2)_{LB}$ subgroup, these matrices are provided in Ref. [13]. g_A and $A_{1\mu}^a$ denote the gauge coupling and field associated with the gauge bosons of $SU(2)_{LA}$. g_B and $A_{2\mu}^a$ represent the gauge coupling and the field associated with $SU(2)_{LB}$, while g_Y and B_μ^3 denote the hypercharge and the field. When Σ and Δ get their VEVs, the gauge fields $A_{1\mu}^a$ and $A_{2\mu}^a$ are mixed to form a massless triplet $A_{0\mu}^a$ and a massive triplet $A_{H\mu}^a$,

$$A_{0\mu}^a = \cos \theta_g A_{1\mu}^a + \sin \theta_g A_{2\mu}^a, \quad A_{H\mu}^a = \sin \theta_g A_{1\mu}^a - \cos \theta_g A_{2\mu}^a, \quad (40)$$

with the mixing angle

$$s_g \equiv \sin \theta_g = \frac{g_A}{\sqrt{g_A^2 + g_B^2}}, \quad c_g \equiv \cos \theta_g = \frac{g_B}{\sqrt{g_A^2 + g_B^2}}, \quad (41)$$

which are related to the electroweak gauge coupling g through

$$g = \frac{g_A g_B}{\sqrt{g_A^2 + g_B^2}}. \quad (42)$$

On the other hand, the weak mixing angle is defined as

$$s_W \equiv \sin \theta_W = \frac{g_Y}{\sqrt{g^2 + g_Y^2}}, \quad c_W \equiv \cos \theta_W = \frac{g}{\sqrt{g^2 + g_Y^2}}. \quad (43)$$

In the BLHM, the masses of the gauge bosons (γ , Z , W^\pm , Z' , W'^\pm) are also generated:

$$m_\gamma^2 = 0, \quad (44)$$

$$m_Z^2 = \frac{1}{4} (g^2 + g_Y^2) v^2 \left(1 - \frac{v^2}{12f^2} \left(2 + \frac{3f^2}{f^2 + F^2} (s_g^2 - c_g^2)^2 \right) \right), \quad (45)$$

$$m_{W^\pm}^2 = \frac{1}{4} g^2 v^2 \left(1 - \frac{v^2}{12f^2} \left(2 + \frac{3f^2}{f^2 + F^2} (s_g^2 - c_g^2)^2 \right) \right), \quad (46)$$

$$m_{Z'}^2 = m_{W'^\pm}^2 + \frac{g^2 s_W^2 v^4}{16c_W^2 (f^2 + F^2)} (s_g^2 - c_g^2)^2, \quad (47)$$

$$m_{W'^\pm}^2 = \frac{g^2}{4c_g^2 s_g^2} (f^2 + F^2) - m_{W^\pm}^2. \quad (48)$$

C. The Yang-Mills sector

The gauge boson self-interactions arise from the following Lagrangian terms:

$$\mathcal{L} = F_{1\mu\nu}F_1^{\mu\nu} + F_{2\mu\nu}F_2^{\mu\nu}, \quad (49)$$

where $F_{1,2}^{\mu\nu}$ are given explicitly as

$$F_1^{\mu\nu} = \partial^\mu A_1^{\alpha\nu} - \partial^\nu A_1^{\alpha\mu} + g_A \sum_b \sum_c \epsilon^{abc} A_1^{b\mu} A_1^{c\nu}, \quad (50)$$

$$F_2^{\mu\nu} = \partial^\mu A_2^{\alpha\nu} - \partial^\nu A_2^{\alpha\mu} + g_B \sum_b \sum_c \epsilon^{abc} A_2^{b\mu} A_2^{c\nu}. \quad (51)$$

The indices a , b , and c run over the three gauge fields [31]; ϵ^{abc} is the anti-symmetric tensor.

D. The fermion sector

In the BLHM, the fermionic sector is divided into two parts. First, the Lagrangian of Eq. (52) represents the massive fermion sector. This sector includes the top and bottom quarks of the SM and a series of new quarks arranged in four multiplets: Q and Q' , which transform under $SO(6)_A$, while U^c and U_5^c transform under the group $SO(6)_B$. Second, the sector of light fermions contained in Eq. (61), in this expression, all the interactions of the remaining fermions of the SM with the exotic particles of the BLHM are generated.

For massive fermions, the Lagrangian that describes them is given by [13]

$$\mathcal{L}_t = y_1 f Q^T S \Sigma S U^c + y_2 f Q'^T \Sigma U^c + y_3 f Q'^T \Sigma U_5^c + y_b f q_3^T (-2iT_R^2 \Sigma) U_b^c + \text{h.c.}, \quad (52)$$

where $S = \text{diag}(1, 1, 1, 1, -1, -1)$. The explicit representation of the multiplets involved in Eq. (52) are arranged as follows

$$Q^T = \frac{1}{\sqrt{2}} ((-Q_{a_1} - Q_{b_2}), i(Q_{a_1} - Q_{b_2}), (Q_{a_2} - Q_{b_1}), i(Q_{a_2} - Q_{b_1}), Q_5, Q_6), \quad (53)$$

$$Q'^T = \frac{1}{\sqrt{2}} (-Q'_{a_1}, iQ'_{a_1}, Q'_{a_2}, iQ'_{a_2}, 0, 0), \quad (54)$$

$$q_3^T = \frac{1}{\sqrt{2}} (-\bar{t}_L, i\bar{t}_L, \bar{b}_L, i\bar{b}_L, 0, 0), \quad (55)$$

$$U^{cT} = \frac{1}{\sqrt{2}} ((-U_{b_1}^c - U_{a_2}^c), i(U_{b_1}^c - U_{a_2}^c), (U_{b_2}^c - U_{a_1}^c), i(U_{b_2}^c - U_{a_1}^c), U_5^c, U_6^c), \quad (56)$$

$$U'^{cT} = (0, 0, 0, 0, U_5^c, 0), \quad (57)$$

$$U_b^{cT} = (0, 0, 0, 0, b^c, 0). \quad (58)$$

For simplicity, the Yukawa couplings y_i ($i = 1, 2, 3$) are assumed to be real [13, 18]. These Yukawa couplings can also be written in terms of the Yukawa coupling of the top quark in the following way

$$y_t = \frac{m_t}{v \sin \beta} = \frac{3y_1 y_2 y_3}{\sqrt{(y_1^2 + y_2^2)(y_1^2 + y_3^2)}}. \quad (59)$$

From Eq. (59), it is clear that the top Yukawa coupling is related to the three Yukawa couplings of the model, which, in turn, are part of the fine-tuning measure in the BLHM [13, 29], Ψ , defined as

$$\Psi = \frac{27f^2}{8\pi^2 \lambda_0 v^2 \cos^2 \beta} \frac{|y_1|^2 |y_2|^2 |y_3|^2}{|y_2|^2 - |y_3|^2} \log \left(\frac{|y_1|^2 + |y_2|^2}{|y_1|^2 + |y_3|^2} \right). \quad (60)$$

As for the light fermions, their Lagrangian is

$$\mathcal{L}_{light} = \sum_{i=1,2} y_u f q_i^T \Sigma u_i^c + \sum_{i=1,2} y_d f q_i^T (-2iT_R^2 \Sigma) d_i^c + \sum_{i=1,2,3} y_e f l_i^T (-2iT_R^2 \Sigma) e_i^c + \text{h.c.}, \quad (61)$$

with

$$q_i^T = \frac{1}{\sqrt{2}}(-\bar{u}_{iL}, i\bar{u}_{iL}, \bar{d}_{iL}, i\bar{d}_{iL}, 0, 0), \quad (62)$$

$$l_i^T = \frac{1}{\sqrt{2}}(-\bar{\nu}_{iL}, i\bar{\nu}_{iL}, \bar{e}_{iL}, i\bar{e}_{iL}, 0, 0), \quad (63)$$

$$u_i^{cT} = (0, 0, 0, 0, u_i^c, 0), \quad (64)$$

$$d_i^{cT} = (0, 0, 0, 0, d_i^c, 0), \quad (65)$$

$$e_i^{cT} = (0, 0, 0, 0, e_i^c, 0). \quad (66)$$

Concerning the Yukawa couplings y_f ($f = u, d, e, b$), these are associated with the masses of the fermions as

$$m_f^2 = y_f^2 v^2 \sin^2 \beta \left(1 - \frac{v^2}{3f^2}\right). \quad (67)$$

Since the top quark loops provide the largest divergent corrections to the Higgs mass in the SM, the heavy quark sector in the BLHM scenario is the most crucial for solving the hierarchy problem. The new heavy quarks arising in the BLHM are T , T_5 , T_6 , $T^{2/3}$, $T^{5/3}$, and B , whose associated masses are given as

$$m_T^2 = (y_1^2 + y_2^2)f^2 + \frac{9v_1^2 y_1^2 y_2^2 y_3^2}{(y_1^2 + y_2^2)(y_2^2 - y_3^2)}, \quad (68)$$

$$m_{T_5}^2 = (y_1^2 + y_3^2)f^2 - \frac{9v_1^2 y_1^2 y_2^2 y_3^2}{(y_1^2 + y_3^2)(y_2^2 - y_3^2)}, \quad (69)$$

$$m_{T_6}^2 = m_{T_b^{2/3}}^2 = m_{T_b^{5/3}}^2 = y_1^2 f^2, \quad (70)$$

$$m_B^2 = (y_1^2 + y_2^2)f^2, \quad (71)$$

where $v_1 = v \sin \beta$ and $v_2 = v \cos \beta$. The mass terms for the new quarks, Eqs. (68)-(71), are calculated under the assumption that $y_2 \neq y_3$, otherwise the masses of T and T_5 are degenerate at lowest order [18, 29].

E. The currents sector

The Lagrangian that describes the interactions of fermions with the gauge bosons is [13, 29]

$$\begin{aligned} \mathcal{L} = & \bar{Q}\bar{\tau}^\mu D_\mu Q + \bar{Q}'\bar{\tau}^\mu D_\mu Q' - U^{c\dagger}\tau^\mu D_\mu U^c - U'^{c\dagger}\tau^\mu D_\mu U'^c - U_b^{c\dagger}\tau^\mu D_\mu U_b^c + \sum_{i=1,2} q_i^\dagger\tau^\mu D_\mu q_i \\ & + \sum_{i=1,2,3} l_i^\dagger\tau^\mu D_\mu l_i - \sum_{i=1,2,3} e_i^{c\dagger}\tau^\mu D_\mu e_i^c - \sum_{i=1,2} u_i^{c\dagger}\tau^\mu D_\mu u_i^c - \sum_{i=1,2} d_i^{c\dagger}\tau^\mu D_\mu d_i^c, \end{aligned} \quad (72)$$

where τ^μ and $\bar{\tau}^\mu$ are defined according to Ref. [32]. On the other hand, the covariant derivatives are defined as follows

$$D_\mu Q = \partial_\mu Q + \sum_a (ig_A A_{1\mu}^a T_L^a Q) + ig_Y B_{3\mu} (T_R^3 + T_X^+) Q, \quad (73)$$

$$D_\mu Q' = \partial_\mu Q' + \sum_a (ig_A A_{1\mu}^a T_L^a Q') + ig_Y B_{3\mu} \left(\frac{1}{6}\right) Q', \quad (74)$$

$$D_\mu U^c = \partial_\mu U^c + \sum_a (ig_B A_{2\mu}^a T_L^a U^c) + ig_Y B_{3\mu} (T_R^3 + T_X^-) U^c, \quad (75)$$

$$D_\mu U'^c = \partial_\mu U'^c + ig_Y B_{3\mu} T_X^- U'^c, \quad (76)$$

$$D_\mu U_b^c = \partial_\mu U_b^c + ig_Y B_{3\mu} \left(\frac{1}{3}\right) U_b^c, \quad (77)$$

$$D_\mu q_i = \partial_\mu q_i + \sum_a (ig_A A_{1\mu}^a T_L^a q_i) + ig_Y B_{3\mu} (T_R^3 + T_X^+) q_i, \quad (78)$$

$$D_\mu l_i = \partial_\mu l_i + \sum_a (ig_B A_{2\mu}^a T_L^a l_i) + ig_Y B_{3\mu} T_R^3 l_i, \quad (79)$$

$$D_\mu e_i^c = \partial_\mu e_i^c + ig_Y B_{3\mu} T_X^e e_i^c, \quad (80)$$

$$D_\mu u_i^c = \partial_\mu u_i^c + ig_Y B_{3\mu} T_X^- u_i^c, \quad (81)$$

$$D_\mu d_i^c = \partial_\mu d_i^c + ig_Y B_{3\mu} T_X^d d_i^c. \quad (82)$$

III. THE TOTAL DECAY WIDTH OF THE Z' BOSON

In this section, we determine the total decay width of the Z' boson, which we need to calculate the cross-section of the Higgs-strahlung processes. In the context of the BLHM, the main decay channels of the Z' gauge boson are $Z' \rightarrow f\bar{f}$ ($f = t, b, T, T_5, T_6, T^{2/3}, T^{5/3}, B$), $Z' \rightarrow W^+W^-$, $Z' \rightarrow Zh_0$ and $Z' \rightarrow ZH_0$. Thus, the total decay width $\Gamma_{Z'}$ of the Z' boson can be estimated as follows

$$\Gamma_{Z'} = \sum_f \Gamma_{f\bar{f}} + \Gamma_{WW} + \Gamma_{Zh_0} + \Gamma_{ZH_0}. \quad (83)$$

We provide below the analytical expressions for the partial decay widths of the Z' boson involved in Eq. (83),

$$\begin{aligned} \Gamma(Z' \rightarrow f\bar{f}) &= \frac{N_c m_{Z'}}{4\pi} \sqrt{1 - \frac{4m_f^2}{m_{Z'}^2}} \left[\left(g_V^{Z'ff} \right)^2 \left(1 + 2 \frac{m_f^2}{m_{Z'}^2} \right) \right. \\ &\quad \left. + \left(g_A^{Z'ff} \right)^2 \left(1 - 4 \frac{m_f^2}{m_{Z'}^2} \right) \right], \end{aligned} \quad (84)$$

$$\begin{aligned} \Gamma(Z' \rightarrow W^+W^-) &= - \frac{m_{Z'}}{16\pi} \left(\frac{g_{CW} v^2 x_s}{f^2 + F^2} \right)^2 \sqrt{1 - \frac{4m_W^2}{m_{Z'}^2}} \left[1 + 12 \left(\frac{m_W^2}{m_{Z'}^2} \right) \right. \\ &\quad \left. + 8 \left(\frac{m_{Z'}^2}{m_W^2} \right) - \frac{9}{4} \left(\frac{m_{Z'}^4}{m_W^4} \right) \right], \end{aligned} \quad (85)$$

$$\begin{aligned} \Gamma(Z' \rightarrow Zh_0) &= \frac{g_{Z'Zh_0}^2}{16\pi m_{Z'}} \sqrt{\left[1 - \left(\frac{m_{h_0} + m_Z}{m_{Z'}} \right)^2 \right] \left[1 - \left(\frac{m_{h_0} - m_Z}{m_{Z'}} \right)^2 \right]} \left[\frac{5}{2} + \frac{1}{4} \left(\frac{m_Z^2}{m_{Z'}^2} \right) \right. \\ &\quad \left. + \frac{1}{4} \left(\frac{m_{Z'}^2}{m_Z^2} \right) - \frac{1}{2} \left(\frac{m_{h_0}^2}{m_{Z'}^2} \right) - \frac{1}{2} \left(\frac{m_{h_0}^2}{m_Z^2} \right) + \frac{1}{4} \left(\frac{m_{h_0}^2}{m_{Z'}^2} \right) \left(\frac{m_{h_0}^2}{m_Z^2} \right) \right], \end{aligned} \quad (86)$$

$$\begin{aligned} \Gamma(Z' \rightarrow ZH_0) &= \frac{g_{Z'ZH_0}^2}{16\pi m_{Z'}} \sqrt{\left[1 - \left(\frac{m_{H_0} + m_Z}{m_{Z'}} \right)^2 \right] \left[1 - \left(\frac{m_{H_0} - m_Z}{m_{Z'}} \right)^2 \right]} \left[\frac{5}{2} + \frac{1}{4} \left(\frac{m_Z^2}{m_{Z'}^2} \right) \right. \\ &\quad \left. + \frac{1}{4} \left(\frac{m_{Z'}^2}{m_Z^2} \right) - \frac{1}{2} \left(\frac{m_{H_0}^2}{m_{Z'}^2} \right) - \frac{1}{2} \left(\frac{m_{H_0}^2}{m_Z^2} \right) + \frac{1}{4} \left(\frac{m_{H_0}^2}{m_{Z'}^2} \right) \left(\frac{m_{H_0}^2}{m_Z^2} \right) \right], \end{aligned} \quad (87)$$

where N_c is the color factor ($N_c = 1$ for leptons and $N_c = 3$ for quarks), $g_V^{Z'ff}$ and $g_A^{Z'ff}$ are the vector and axial-vector coupling constants of the Z' boson with the fermions (see Appendix A [33]), and $g_{Z'Zh_0}$ and $g_{Z'ZH_0}$ denote the effective couplings of the Z' and Z bosons to the Higgs bosons h_0 and H_0 whose explicit expressions are given in Appendix A. On the other hand,

$$x_s = \frac{1}{2} \frac{s_g c_g}{c_W} (s_g^2 - c_g^2). \quad (88)$$

IV. THE HIGGS-STRAHLUNG PROCESSES $\mu^+\mu^- \rightarrow (Z, Z') \rightarrow Zh_0, ZH_0$ IN THE BLHM

A. Higgs-strahlung production $\mu^+\mu^- \rightarrow Zh_0$

The Feynman diagrams contributing to the Higgs-strahlung production processes $\mu^+\mu^- \rightarrow (Z, Z') \rightarrow Zh_0$ are shown in Fig. 1. The respective scattering amplitudes are represented by Eqs. (89) and (90),

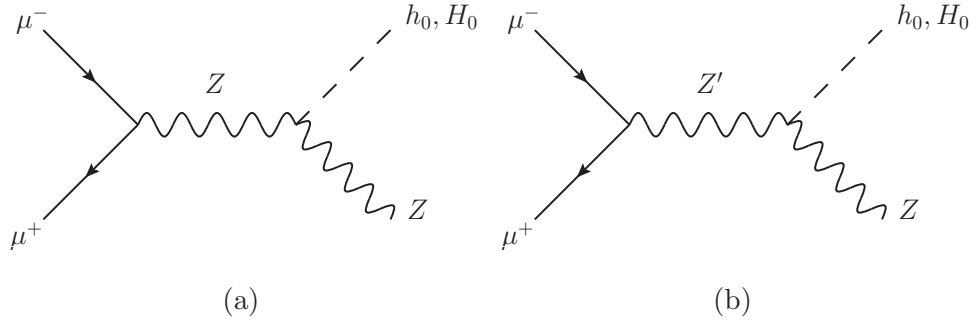


FIG. 1: Feynman diagrams for the Higgs-strahlung production processes a) $\mu^+\mu^- \rightarrow Z \rightarrow Zh_0, ZH_0$ and b) $\mu^+\mu^- \rightarrow Z' \rightarrow Zh_0, ZH_0$ in the BLHM.

$$\begin{aligned} \mathcal{M}_Z(\mu^+\mu^- \rightarrow Zh_0) &= g_{ZZh_0} \left[\bar{v}(p_1) \gamma^\mu (g_V^{Z\mu\mu} - g_A^{Z\mu\mu} \gamma_5) u(p_2) \right] \left[\frac{(-g_{\mu\nu} + p_\mu p_\nu / m_Z^2)}{(p_1 + p_2)^2 - m_Z^2 - im_Z \Gamma_Z} \right] \\ &\times \epsilon'_\lambda(Z), \end{aligned} \quad (89)$$

$$\begin{aligned} \mathcal{M}_{Z'}(\mu^+\mu^- \rightarrow Zh_0) &= g_{ZZ'h_0} \left[\bar{v}(p_1) \gamma^\mu (g_V^{Z'\mu\mu} - g_A^{Z'\mu\mu} \gamma_5) u(p_2) \right] \left[\frac{(-g_{\mu\nu} + p_\mu p_\nu / m_{Z'}^2)}{(p_1 + p_2)^2 - m_{Z'}^2 - im_{Z'} \Gamma_{Z'}} \right] \\ &\times \epsilon'_\lambda(Z), \end{aligned} \quad (90)$$

where $\epsilon'_\lambda(Z)$ represents the polarization vector of the Z boson. The vector and vector-axial coupling constants of the Z or Z' boson are given in Appendix A.

We calculate from the transition amplitudes, Eqs. (89) and (90), the total cross-section $\sigma_T^{Zh_0}$ for the processes $\mu^+\mu^- \rightarrow (Z, Z') \rightarrow Zh_0$,

$$\sigma_T^{Zh_0} = \sigma_Z + \sigma_{Z'} + \sigma_{ZZ'}, \quad (91)$$

with

$$\sigma_Z = \frac{\sqrt{\lambda}}{192\pi} \left(\frac{(g_V^{Z\mu\mu})^2 + (g_A^{Z\mu\mu})^2}{m_Z^2 s^2} \right) \left(\frac{g_{ZZh_0}^2}{(s - m_Z^2)^2 + (m_Z \Gamma_Z)^2} \right) (12m_Z^2 s + \lambda), \quad (92)$$

$$\sigma_{Z'} = \frac{\sqrt{\lambda}}{192\pi} \left(\frac{(g_V^{Z'\mu\mu})^2 + (g_A^{Z'\mu\mu})^2}{m_{Z'}^2 s^2} \right) \left(\frac{g_{Z'Zh_0}^2}{(s - m_{Z'}^2)^2 + (m_{Z'} \Gamma_{Z'})^2} \right) (12m_{Z'}^2 s + \lambda), \quad (93)$$

$$\begin{aligned} \sigma_{ZZ'} &= \sqrt{\lambda} \left(\frac{g_{ZZh_0} g_{Z'Zh_0}}{96\pi} \right) \left(\frac{g_V^{Z\mu\mu} g_V^{Z'\mu\mu} + g_A^{Z\mu\mu} g_A^{Z'\mu\mu}}{m_Z^2 s^2} \right) (12m_Z^2 s + \lambda) \\ &\times \frac{(s - m_Z^2)(s - m_{Z'}^2) + (m_Z \Gamma_Z)(\Gamma_{Z'} m_{Z'})}{((m_Z^2 - s)^2 + (m_Z \Gamma_Z)^2)((m_{Z'}^2 - s)^2 + (m_{Z'} \Gamma_{Z'})^2)}, \end{aligned} \quad (94)$$

where σ_Z and $\sigma_{Z'}$ are the cross-sections of processes $\mu^+ \mu^- \rightarrow Z \rightarrow Zh_0$ and $\mu^+ \mu^- \rightarrow Z' \rightarrow Zh_0$, respectively. The $\sigma_{ZZ'}$ cross-section represents the interference term between the Z and Z' bosons. In Eqs. (92)-(94), \sqrt{s} is the center-of-mass energy and λ is the usual two-particle phase space function,

$$\lambda(s, m_Z, m_{h_0}) = (s - m_Z^2 - m_{h_0}^2)^2 - 4m_Z^2 m_{h_0}^2. \quad (95)$$

It is appropriate to mention that Eq. (91), which corresponds to the total cross-section in the context of the BLHM, reproduces the cross-section for the process $\mu^+ \mu^- \rightarrow Z \rightarrow Zh_0$ obtained in the SM scenario [34–39]. This is reached in the decoupling limit of the new physics scales, i.e., $(f, F) \rightarrow \infty$.

To quantify the combined effects of the free parameters \sqrt{s} , f and F of the BLHM, we define the relative correction for the total cross-section as follows,

$$\frac{\delta\sigma^{BLHM}}{\sigma^{SM}} = \frac{\sigma_T^{Zh_0}(\sqrt{s}, f, F) - \sigma^{SM}(\sqrt{s})}{\sigma^{SM}(\sqrt{s})}, \quad (96)$$

where $\sigma^{SM}(\sqrt{s})$ represent the cross-section of the SM and $\sigma_T^{Zh_0}(\sqrt{s}, f, F)$ represent the cross-section in the presence of interactions of the BLHM.

B. Higgs-strahlung production $\mu^+ \mu^- \rightarrow ZH_0$

We determine the scattering amplitudes and cross-sections of Higgs-strahlung production $\mu^+ \mu^- \rightarrow (Z, Z') \rightarrow ZH_0$. The transition amplitudes are obtained from the Feynman diagrams contributing to the process $\mu^+ \mu^- \rightarrow ZH_0$ (see Fig. 1), which are given by

$$\begin{aligned} \mathcal{M}_Z(\mu^+\mu^- \rightarrow ZH_0) &= g_{ZZH_0} \left[\bar{v}(p_1)\gamma^\mu(g_V^{Z\mu\mu} - g_A^{Z\mu\mu}\gamma_5)u(p_2) \right] \left[\frac{(-g_{\mu\nu} + p_\mu p_\nu/m_Z^2)}{(p_1 + p_2)^2 - m_Z^2 - im_Z\Gamma_Z} \right] \\ &\times \epsilon_\lambda^\nu(Z), \end{aligned} \quad (97)$$

$$\begin{aligned} \mathcal{M}_{Z'}(\mu^+\mu^- \rightarrow ZH_0) &= g_{ZZ'H_0} \left[\bar{v}(p_1)\gamma^\mu(g_V^{Z'\mu\mu} - g_A^{Z'\mu\mu}\gamma_5)u(p_2) \right] \left[\frac{(-g_{\mu\nu} + p_\mu p_\nu/m_{Z'}^2)}{(p_1 + p_2)^2 - m_{Z'}^2 - im_{Z'}\Gamma_{Z'}} \right] \\ &\times \epsilon_\lambda^\nu(Z). \end{aligned} \quad (98)$$

Using Eqs. (97) and (98), we calculate the total cross-section for the process $\mu^+\mu^- \rightarrow (Z, Z') \rightarrow ZH_0$, which can be written in the following compact form,

$$\sigma_T^{ZH_0} = \sigma_Z + \sigma_{Z'} + \sigma_{ZZ'}, \quad (99)$$

where

$$\sigma_Z = \frac{\sqrt{\lambda}}{192\pi} \left(\frac{(g_V^{Z\mu\mu})^2 + (g_A^{Z\mu\mu})^2}{m_Z^2 s^2} \right) \left(\frac{g_{ZZH_0}^2}{(s - m_Z^2)^2 + (m_Z\Gamma_Z)^2} \right) (12m_Z^2 s + \lambda), \quad (100)$$

$$\sigma_{Z'} = \frac{\sqrt{\lambda}}{192\pi} \left(\frac{(g_V^{Z'\mu\mu})^2 + (g_A^{Z'\mu\mu})^2}{m_{Z'}^2 s^2} \right) \left(\frac{g_{Z'ZH_0}^2}{(s - m_{Z'}^2)^2 + (m_{Z'}\Gamma_{Z'})^2} \right) (12m_{Z'}^2 s + \lambda), \quad (101)$$

$$\begin{aligned} \sigma_{ZZ'} &= \sqrt{\lambda} \left(\frac{g_{ZZH_0}g_{Z'ZH_0}}{96\pi} \right) \left(\frac{g_V^{Z\mu\mu}g_V^{Z'\mu\mu} + g_A^{Z\mu\mu}g_A^{Z'\mu\mu}}{m_Z^2 s^2} \right) (12m_Z^2 s + \lambda) \\ &\times \frac{(s - m_Z^2)(s - m_{Z'}^2) + (m_Z\Gamma_Z)(m_{Z'}\Gamma_{Z'})}{((m_Z^2 - s)^2 + (m_Z\Gamma_Z)^2)((m_{Z'}^2 - s)^2 + (m_{Z'}\Gamma_{Z'})^2)}. \end{aligned} \quad (102)$$

In these expressions, the two-particle phase space function is given by

$$\lambda(s, m_Z, m_{H_0}) = (s - m_Z^2 - m_{H_0}^2)^2 - 4m_Z^2 m_{H_0}^2. \quad (103)$$

V. NUMERICAL RESULTS

In our numerical analysis of the Higgs-strahlung production processes $\mu^+\mu^- \rightarrow Zh_0, ZH_0$, various LHC measurements are used to constrain specific relevant parameters of the BLHM. Below, we summarise the different input parameters, searches, and measurements used for our analysis.

As discussed in Refs. [18, 22, 24], the Yukawa couplings, y_1 , y_2 , and y_3 are directly related to the generation of the heavy quark partner masses in the context of the BLHM. These

Yukawa couplings generate two study scenarios, which arise because in the region where $y_2 \approx y_3$, the masses of the T and T_5 quarks are degenerate to the lowest order (see Eqs. (68)-(69)). Consequently, different diagonalization schemes are required for the fermion mass matrix when $y_2 \approx y_3$ versus $|y_2 - y_3| > 0$. The two study scenarios to which we refer are

- Scenario **a** ($y_2 > y_3$), $y_1 = 0.61$, $y_2 = 0.84$ and $y_3 = 0.35$ [22–24],
- Scenario **b** ($y_2 < y_3$), $y_1 = 0.61$, $y_2 = 0.35$ and $y_3 = 0.84$ [22–24].

In the first scenario ($y_2 > y_3$), the mass splitting between the new quarks T_5 and T_6 is relatively tiny and leads to the decays of T_5 being predominantly to SM particles. For the second scenario ($y_2 < y_3$), the mass splitting between T_5 and T_6 is large, which increases the decay modes available for the T_5 quark through decay cascades to non-SM particles [18, 29]. Because of the phenomenological implications of the first scenario, in this paper we explore the Higgs-strahlung production $\mu^+\mu^- \rightarrow Zh_0, ZH_0$ in the $y_2 > y_3$ scenario. On the other hand, our choice in the values of y_i is motivated by the perturbativity requirements [40] and the fine-tuning measure [13, 18]. Using numerical methods, from Eq. (59), we randomize perturbative values of the Yukawa couplings y_i ($i = 1, 2, 3$) by fixing y_t through experimental measurement of the top quark mass ($m_t = 172.69$ GeV [34]) and the Higgs boson mass ($m_{h_0} = 125.25$ GeV [34]), and an appropriate choice of the other parameters involved (m_{A_0} , $\tan\beta$, and others), as discussed below.

The pseudoscalar mass A_0 : This parameter is fixed around 1000 GeV, which is consistent with the current search results for new scalar bosons [41, 42]. According to data recorded by the ATLAS experiment at the LHC, it corresponds to an integrated luminosity of 139 fb^{-1} from pp collisions at center-of-mass energy 13 TeV were used to search for a heavy Higgs boson, A_0 , decaying into ZH_0 , where H_0 denotes another Higgs boson with mass $m_{H_0} > 125$ GeV.

The mass of the Higgs boson H_0 : The Higgs boson mass H_0 in the context of the BLHM is determined from Eq. (35), therefore it has a direct dependence on m_{A_0} .

The ratio of the VEVs v_1 and v_2 , $\tan\beta$: A lower bound emerges for $\tan\beta$ when examining the radiative corrections to m_1 and m_2 in the BLHM, which suggests that $\tan\beta > 1$ [13]. On the other hand, the authors of Ref. [17] set an upper bound to $\tan\beta$ that arises due to perturbativity requirements on the parameter λ_0 . Thus, the range of values that

the parameter $\tan\beta$ could acquire is set according to Eq. (30). Using this expression, when $m_{A_0} = 1000$ GeV, it is obtained that $1 < \tan\beta < 10.45$. Consistently, in this work, we have chosen $\tan\beta = 3$ [22–24] to carry out our numerical analysis of the production of Zh_0 and ZH_0 at a future muon collider.

The gauge couplings, $g_{A,B}$: The gauge couplings g_A and g_B , associated with the $SU(2)_{LA}$ and $SU(2)_{LB}$ gauge bosons, are parametrized in a more phenomenological fashion in terms of a mixing angle θ_g and the $SU(2)_L$ gauge coupling: $\tan\theta_g = g_A/g_B$ and $g = g_A g_B / \sqrt{g_A^2 + g_B^2}$. For our study, it is assumed that the gauge coupling $g_B = \frac{1}{2}g_A$, implies that $g_A = \sqrt{5}g$.

Symmetry breaking scales, f and F : The BLHM features a global $SO(6)_A \times SO(6)_B$ symmetry that is broken to a diagonal $SO(6)_V$ at a scale $f \sim \mathcal{O}(\text{TeV})$ when the non-linear sigma field, Σ , develop a VEV. Bounds on the f scale arise when considering fine-tuning constraints on the heavy quark masses and experimental constraints on heavy quark production. Refs. [17] and [18] establish that $f \in [700, 3000]$ GeV. A second global symmetry of the $SU(2)_C \times SU(2)_D$ form is also present in the BLHM, and is broken to a diagonal $SU(2)$ at a scale $F > f$ when a second non-linear sigma field, Δ , develops a VEV. The energy scale F acquires sufficiently large values compared to the f scale. The purpose is to ensure that the new gauge bosons are much heavier than the new quarks. In this way, $F > 3000$ GeV [13, 17].

One of the motivations for building the BLHM, is to avoid fine-tuning the Higgs potential. In this way, scenarios **a** and **b** mentioned above offer realistic values of the Yukawa couplings as they satisfy the perturbativity requirements and minimize the fine-tuning constraints as the energy scale f takes on values close to 3000 GeV. From Eq. (60), we determine the fine-tuning measurement as the new physics f scale takes specific values in the 1000 to 3000 GeV range. In Table I, we show a measure of the fine-tuning when the energy scale f takes on values such as 1.0, 1.5, 2.0, 2.5, and 3.0 TeV. According to the numerical values listed in Table I, the size of the fine-tuning when $f = 1.0$ TeV is $\Psi = 0.54$, which indicates that there is no fine-tuning in the BLHM [13, 29]. The absence of fine-tuning prevails up to $\Psi = 2.2$, i.e., for values of the energy scale f close to 2 TeV. The fine-tuning starts to become significant for $f > 2.1$ TeV.

TABLE I: A measure of the fine-tuning in the BLHM for some values of the f scale.

f [TeV]	Ψ
1.0	0.54
1.5	1.21
2.0	2.16
2.5	3.37
3.0	4.85

As a summary, we provide in Table II the values assigned to the parameters involved in our calculation.

TABLE II: Values assigned to the parameters involved in our numerical analysis at the BLHM.

Parameter	Value	Reference
m_{h_0}	125.25 GeV	[34]
m_{A_0}	1000 GeV	[41, 42]
$\tan \beta$	3	[22–24]
m_{H_0}	1015 GeV	
g_A	$\sqrt{5} g$	
Γ_Z	2.4952 ± 0.0023 GeV	[34]
f	[1000, 3000] GeV	[13, 18, 22–24]
F	> 3000 GeV	[13, 17, 18, 22–24]

A. $\Gamma_{Z'}$

Another of the essential input parameters involved in our study of the Higgs-strahlung production $\mu^+\mu^- \rightarrow (Z, Z') \rightarrow Zh_0, ZH_0$ is the total decay width of the Z' boson ($\Gamma_{Z'}$), which has a dependence on the two energy scales, f and F , these represent the scales of the new physics in the BLHM. In this subsection, we analyze the different contributions that receive $\Gamma_{Z'}$, and we also discuss the behavior of the partial widths $\Gamma(Z' \rightarrow X)$ when

the f scale takes values from 1000 to 3000 GeV while keeping the F scale fixed, and when F varies from 4000 to 6000 GeV while fixing f (see Fig. 2). In the left plot of Fig. 2, we show the evolution of $\Gamma(Z' \rightarrow X)$ vs. f ; these curves are generated by setting $F = 6000$ GeV. In this scenario, the main partial contributions are generated by the decays $Z' \rightarrow T^{2/3}\bar{T}^{2/3}$ and $Z' \rightarrow T\bar{T}$. These provide the dominant and subdominant numerical contributions: $\Gamma(Z' \rightarrow T^{2/3}\bar{T}^{2/3}) = [262.43, 256.61]$ GeV and $\Gamma(Z' \rightarrow T\bar{T}) = [259.70, 249.83]$ GeV, respectively. This occurs while $f \in [1000, 1650]$ GeV, outside this interval, $\Gamma(Z' \rightarrow t\bar{t})$ becomes dominant. On the opposite side, the most suppressed contribution is given by the $Z' \rightarrow ZH_0$ decay: $\Gamma(Z' \rightarrow ZH_0) = [9.27 \times 10^{-3}, 1.07 \times 10^{-2}]$ GeV over the whole analysis interval of the f scale. With respect to the remaining curves, $\Gamma(Z' \rightarrow T^{5/3}\bar{T}^{5/3}) \approx \Gamma(Z' \rightarrow B\bar{B}) \approx \Gamma(Z' \rightarrow b\bar{b}) \in [2.60, 1.35] \times 10^2$ GeV, $\Gamma(Z' \rightarrow WW) \approx \Gamma(Z' \rightarrow Zh_0) \in [6.0, 2.3] \times 10^1$ GeV, and $\Gamma(Z' \rightarrow T_5\bar{T}_5) \approx \Gamma(Z' \rightarrow T_6\bar{T}_6) \in [10^{-1}, 10^{-3}]$ GeV. On the other hand, in the right plot of Fig. 2, we can appreciate the behavior of $\Gamma(Z' \rightarrow X)$ vs. F , these curves have been generated for $f = 1000$ GeV. In this case, the most significant contributions are given by the decays $Z' \rightarrow T^{2/3}\bar{T}^{2/3}$ and $Z' \rightarrow T\bar{T}$: $\Gamma(Z' \rightarrow T^{2/3}\bar{T}^{2/3}) = [172.99, 262.43]$ GeV and $\Gamma(Z' \rightarrow T\bar{T}) = [169.08, 259.70]$ GeV when the F scale obtains values in the interval from 4000 to 6000 GeV. On the contrary, the minor contribution is led by the process $Z' \rightarrow ZH_0$, $\Gamma(Z' \rightarrow ZH_0) = [5.39, 9.27] \times 10^{-3}$ GeV. The other curves approximately take on values in the following ranges: $\Gamma(Z' \rightarrow t\bar{t}) \approx \Gamma(Z' \rightarrow T^{5/3}\bar{T}^{5/3}) \approx \Gamma(Z' \rightarrow B\bar{B}) \in [1.0, 2.5] \times 10^2$ GeV, $\Gamma(Z' \rightarrow b\bar{b}) \approx \Gamma(Z' \rightarrow WW) \approx \Gamma(Z' \rightarrow Zh_0) \in [0.9 \times 10^2, 1.0 \times 10^1]$ GeV, and $\Gamma(Z' \rightarrow T_5\bar{T}_5) \approx \Gamma(Z' \rightarrow T_6\bar{T}_6) \sim 10^{-1}$ GeV. From the above, $\Gamma(Z' \rightarrow X)$ shows a strong sensitivity to variations in the scales of the new physics (f and F), and the most significant contributions to $\Gamma_{Z'}$ are generated due to fermions.

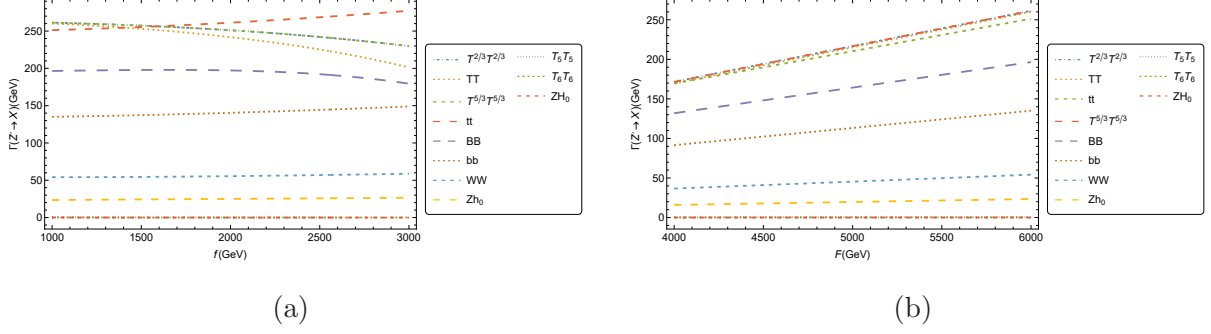


FIG. 2: Decay widths for the processes $Z' \rightarrow X$ where $X = t\bar{t}, T\bar{T}, T_5\bar{T}_5, T_6\bar{T}_6, T^{2/3}\bar{T}^{2/3}, T^{5/3}\bar{T}^{5/3}, b\bar{b}, B\bar{B}, Zh_0, ZH_0, WW$. a) $\Gamma(Z' \rightarrow X)$ as a function of the f energy scale (with the fixed value of $F = 6\,000$ GeV). b) $\Gamma(Z' \rightarrow X)$ as a function of the F energy scale (with the fixed value of $f = 1\,000$ GeV).

B. $\text{Br}(Z' \rightarrow X)$

We now present our results on the branching ratios of the Z' gauge boson as a function of the scales of new physics (f or F). We first discuss the behavior observed in Fig. 3(a). In this figure, we plot $\text{Br}(Z' \rightarrow X)$ vs. the f scale while fixing the second F scale at 6000 GeV. The curve that provides the dominant contribution is given by the $Z' \rightarrow T^{2/3}\bar{T}^{2/3}$ decay, its associated branching ratio is $\text{Br}(Z' \rightarrow T^{2/3}\bar{T}^{2/3}) = [1.80, 1.68] \times 10^{-1}$ when $f \in [1\,000, 3\,000]$ GeV. On the opposite side, we find that the $Z' \rightarrow ZH_0$ decay provides the most suppressed contribution, $\text{Br}(Z' \rightarrow ZH_0) = [6.35, 7.85] \times 10^{-6}$. As far as the remaining branching ratios are concerned, these acquire values of $\text{Br}(Z' \rightarrow T\bar{T}) \sim \text{Br}(Z' \rightarrow t\bar{t}) \sim \text{Br}(Z' \rightarrow T^{5/3}\bar{T}^{5/3}) \sim \text{Br}(Z' \rightarrow B\bar{B}) \sim 10^{-1}$, $\text{Br}(Z' \rightarrow b\bar{b}) \sim \text{Br}(Z' \rightarrow Zh_0) \sim \text{Br}(Z' \rightarrow WW) \sim 10^{-1} - 10^{-2}$, and $\text{Br}(Z' \rightarrow T_5\bar{T}_5) \sim \text{Br}(Z' \rightarrow T_6\bar{T}_6) \sim 10^{-4} - 10^{-6}$. Concerning Fig. 3(b), here we explore the behavior of $\text{Br}(Z' \rightarrow X)$ vs. the F scale in the interval from 4000 to 6000 GeV, and all the curves shown in the figure have been generated with the fixed value of $f = 1\,000$ GeV. In this scenario, we can appreciate that the curve that provides the slightly more significant contribution is derived from the $Z' \rightarrow T^{2/3}\bar{T}^{2/3}$ decay, $\text{Br}(Z' \rightarrow T^{2/3}\bar{T}^{2/3}) = [1.79, 1.80] \times 10^{-1}$. On the other hand, the smallest contribution is given by $\text{Br}(Z' \rightarrow ZH_0) = [5.58, 6.35] \times 10^{-6}$. The decays $Z' \rightarrow T\bar{T}$, $Z' \rightarrow t\bar{t}$, $Z' \rightarrow T^{5/3}\bar{T}^{5/3}$ and $Z' \rightarrow B\bar{B}$ also generate branching ratios with values of the same order of magnitude than the main contribution although slightly smaller. Complementarily, the other branching ratios acquire

values of $\text{Br}(Z' \rightarrow b\bar{b}) \sim \text{Br}(Z' \rightarrow WW) \sim \text{Br}(Z' \rightarrow Zh_0) \sim 10^{-2}$, $\text{Br}(Z' \rightarrow T_5\bar{T}_5) \sim 10^{-4}$ and $\text{Br}(Z' \rightarrow T_6\bar{T}_6) \sim 10^{-5}$. In conclusion, the values obtained by the branching ratios $\text{Br}(Z' \rightarrow X)$ do not show appreciable changes as the F scale increases to 6000 GeV, as shown in the corresponding figure. $\text{Br}(Z' \rightarrow X)$ slightly depends on the F scale compared to the f scale.

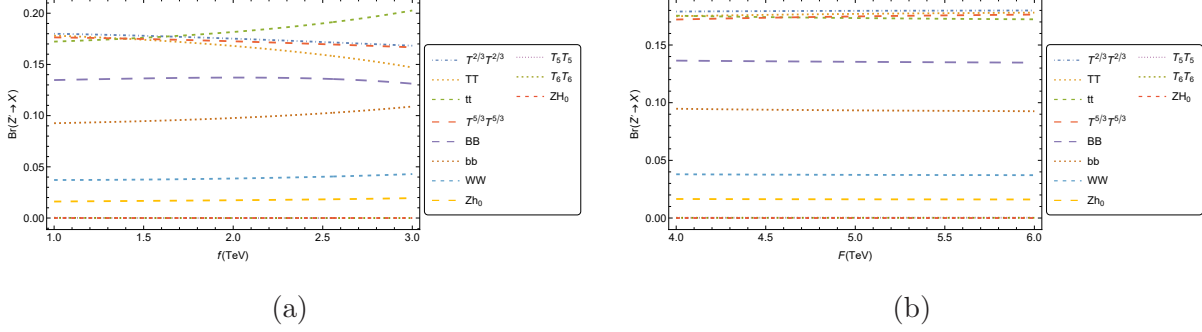


FIG. 3: The branching ratios for the processes $Z' \rightarrow X$ where $X = t\bar{t}, T\bar{T}, T_5\bar{T}_5, T_6\bar{T}_6, T^{2/3}\bar{T}^{2/3}, T^{5/3}\bar{T}^{5/3}, b\bar{b}, B\bar{B}, Zh_0, ZH_0, WW$. a) $\text{Br}(Z' \rightarrow X)$ as a function of the f energy scale (with the fixed value of $F = 6000$ GeV). b) $\text{Br}(Z' \rightarrow X)$ as a function of the F energy scale (with the fixed value of $f = 1000$ GeV).

C. Higgs boson production h_0 in the BLHM

We investigate the Higgs-strahlung production process $\mu^+\mu^- \rightarrow Zh_0$ at the future muon collider and calculate the BLHM predictions on the $\sigma_T^{Zh_0}(\sqrt{s}, f, F)$ cross-section. We scan the BLHM parameters by considering various experimental and theoretical constraints. In Fig. 4, we present our results for the total cross-section $\sigma_T^{Zh_0}(\mu^+\mu^- \rightarrow Zh_0)$ where the resonant and non-resonant effects of the processes $\mu^+\mu^- \rightarrow (Z, Z') \rightarrow Zh_0$ are taken into account. We also show the different contributions received by $\sigma_T^{Zh_0}(\mu^+\mu^- \rightarrow Zh_0)$ according to Eq. (91): $\sigma_Z(\mu^+\mu^- \rightarrow Zh_0)$, $\sigma_{Z'}(\mu^+\mu^- \rightarrow Zh_0)$, and $\sigma_{ZZ'}(\mu^+\mu^- \rightarrow Zh_0)$. Complementarily, we plot in this same scenario the contribution of the SM represented by $\sigma_{SM}(\mu^+\mu^- \rightarrow Zh_0)$. From Fig. 4, we can appreciate that the behavior of the cross-section $\sigma_{SM}(\mu^+\mu^- \rightarrow Zh_0)$ very closely resembles the behavior of the curve represented by $\sigma_Z(\mu^+\mu^- \rightarrow Zh_0)$. The latter corresponds to the cross-section with the Z boson exchange in the context of the BLHM. In this particular case, the contribution of new physics is almost negligible. Concerning the other curves, $\sigma_{Z'}$ and $\sigma_T (\equiv \sigma_T^{Zh_0})$, these obtain an increase in the

cross-section for large values of the center-of-mass energy, reaching their maximum value at the resonance of the Z' gauge boson, i.e., when $\sqrt{s} \approx 5\,200$ GeV: $\sigma_{Z'}(\mu^+\mu^- \rightarrow Zh_0) = 3.72$ fb, and $\sigma_T(\mu^+\mu^- \rightarrow Zh_0) = 4.04$ fb. For this benchmark, $\sigma_{ZZ'}(\mu^+\mu^- \rightarrow Zh_0)$ its contribution is 0.64 fb.

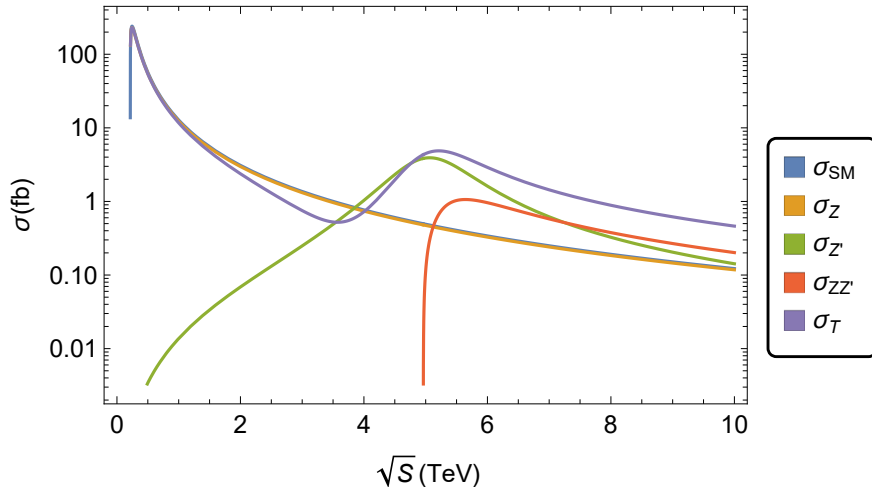


FIG. 4: The cross-section of the process $\mu^+\mu^- \rightarrow (Z, Z') \rightarrow Zh_0$ as a function of \sqrt{s} . The curves are generated for $f = 1000$ GeV and $F = 6000$ GeV (for $m_{Z'} = 5\,200$ GeV), and correspond to σ_{SM} , σ_Z (Eq. (92)), $\sigma_{Z'}$ (Eq. (93)), $\sigma_{ZZ'}$ (Eq. (94)), and $\sigma_T \equiv \sigma_T^{Zh_0}$ (Eq. (91)).

We test through the total cross-section the effects that could be provided by the new physics scales, f and F , on $\sigma_T(\mu^+\mu^- \rightarrow Zh_0)$. In this way, in Fig. 5 we show the different curves generated for $\sigma_T(\mu^+\mu^- \rightarrow Zh_0)$ when the f and F scales take specific fixed values while the center-of-mass energy \sqrt{s} varies in the interval from 0 to 10 000 GeV. In this figure, we can see that the curves corresponding to $\sigma_T(\mu^+\mu^- \rightarrow Zh_0)$ decrease for large values of \sqrt{s} . We also note that the height of the resonance peaks for the Z' boson changes depending on the value of the F scale. For the plotted curves, $\sigma_T(\mu^+\mu^- \rightarrow Zh_0)$ reaches its local maxima just at the resonance of the Z' gauge boson: $\sigma_T(\sqrt{s}, 1\,000 \text{ GeV}, 4\,000 \text{ GeV}) = 10.99$ fb, $\sigma_T(\sqrt{s}, 1\,000 \text{ GeV}, 5\,000 \text{ GeV}) = 7.02$ fb and $\sigma_T(\sqrt{s}, 1\,000 \text{ GeV}, 6\,000 \text{ GeV}) = 4.87$ fb for $m_{Z'} \approx 3\,500$ GeV, $m_{Z'} \approx 4\,300$ GeV and $m_{Z'} \approx 5\,200$ GeV, respectively. It is essential to mention that in the context of the BLHM, the mass of the Z' gauge boson depends on the scales of the new model physics, f and F (see Eq. (47)). From the above, the total cross-section $\sigma_T(\sqrt{s}, f, F)$ is sensitive to changes in the free parameters. Contributions

from new physics show remarkable effects concerning the SM contribution; the region of most significant appreciation of such effects is for $\sqrt{s} \in [800, 10\,000]$ GeV.

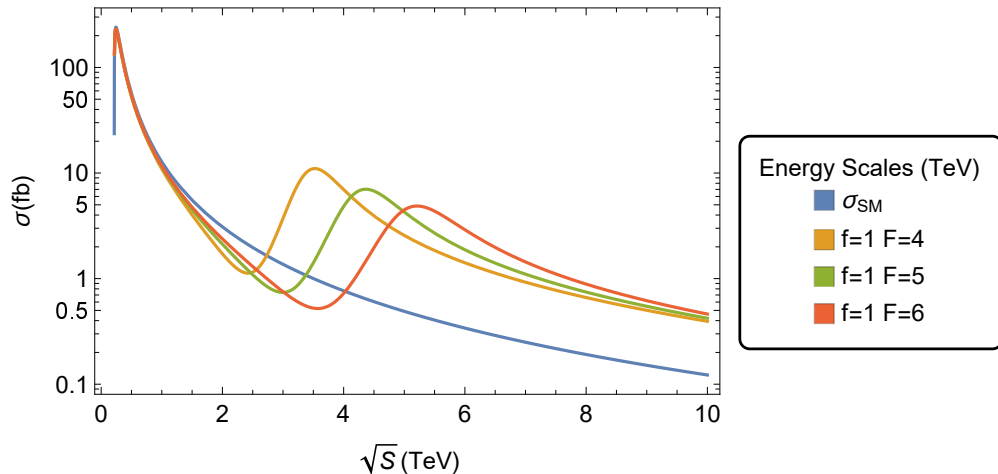


FIG. 5: The total cross-section of the process $\mu^+\mu^- \rightarrow (Z, Z') \rightarrow Zh_0$ as a function of \sqrt{s} . The curves are generated for $f = 1000$ GeV and $F = 4000$ GeV, $f = 1000$ GeV and $F = 5000$ GeV, and $f = 1000$ GeV and $F = 6000$ GeV.

The BLHM can generate corrections to the production cross-section for the process $\mu^+\mu^- \rightarrow Zh_0$ via modification of the tree-level ZZh_0 coupling, as well as by the new interaction vertex $Z'Zh_0$. The values of the relative corrections are calculated from Eq. (96). In Fig. 6, we show the relative corrections $\frac{\delta\sigma_{BLHM}}{\sigma_{SM}}$ of the Higgs-strahlung process $\mu^+\mu^- \rightarrow Zh_0$ as a function of \sqrt{s} for $f = 1000$ GeV and $F = 4000$ GeV, $f = 1000$ GeV and $F = 5000$ GeV, and $f = 1000$ GeV and $F = 6000$ GeV. In this figure, the absolute value of the relative correction increases for smaller values of the energy scale F and decouples at high scales of the \sqrt{s} parameter. The values of $|\frac{\delta\sigma_{BLHM}}{\sigma_{SM}}|$ are in the ranges of 0% – 10% in most of the parameter space. Our numerical results show that for reasonable values of the free parameters of the BLHM, \sqrt{s} , f and F , can generate significant contributions to the total cross-section of the Higgs-strahlung process $\mu^+\mu^- \rightarrow Zh_0$ concerning their value in the context of the SM.

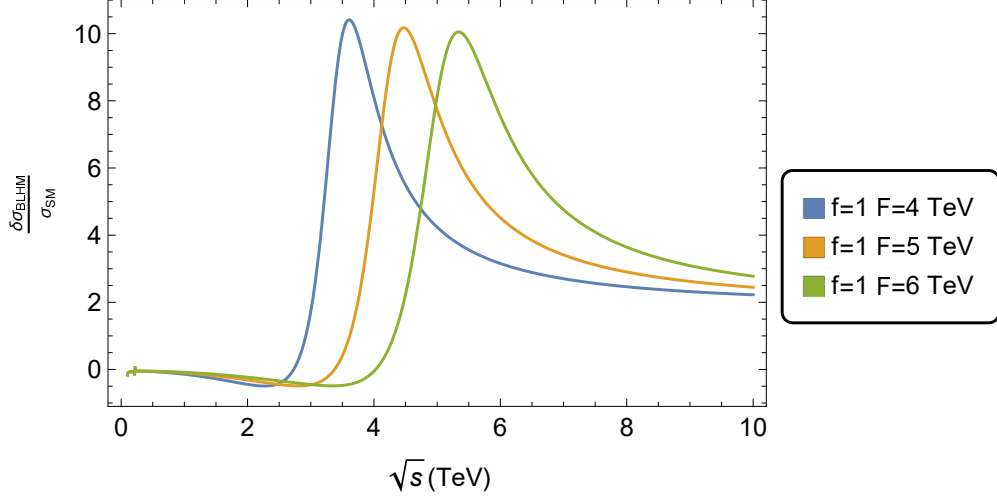


FIG. 6: Relative correction $\frac{\delta\sigma_{BLHM}}{\sigma_{SM}}$ as a function of the center-of-mass energy \sqrt{s} .

We also discuss the production of Zh_0 at the future muon collider, assuming design luminosities $\mathcal{L} = 2, 4, 6, 10, 30 \text{ ab}^{-1}$ and center-of-mass energies, $\sqrt{s} = 3, 4, 5, 6, 7, 10, 30 \text{ TeV}$ [19, 43, 44]. In Tables III and IV for $f = 1000 \text{ GeV}$ and $F = 4000 \text{ GeV}$, and $f = 1000 \text{ GeV}$ and $F = 6000 \text{ GeV}$, respectively, we present an event estimate of the production associated to Zh_0 . According to the numerical results, around the resonance of the Z' gauge boson, the number of Zh_0 events reaches high values. In general, the possibility of being observed in the process $\mu^+\mu^- \rightarrow (Z, Z') \rightarrow Zh_0$ is quite promising at the future muon collider.

TABLE III: The total production of Zh_0 at the future muon collider in the context of the BLHM with $f = 1000 \text{ GeV}$ and $F = 4000 \text{ GeV}$ ($m_{Z'} = 3500 \text{ GeV}$).

$f = 1000 \text{ GeV}, F = 4000 \text{ GeV}$					
$\sqrt{s} \text{ TeV}$	$\mathcal{L} = 2 \text{ ab}^{-1}$	$\mathcal{L} = 4 \text{ ab}^{-1}$	$\mathcal{L} = 6 \text{ ab}^{-1}$	$\mathcal{L} = 10 \text{ ab}^{-1}$	$\mathcal{L} = 30 \text{ ab}^{-1}$
3	7 405	14 810	22 215	37 026	111 079
4	13 882	27 764	41 646	69 410	208 231
5	5 123	10 247	15 371	25 618	76 855
6	2 822	5 645	8 468	14 113	42 341
7	1 847	3 694	5 541	9 235	27 705
10	787	1 575	2 363	3 938	11 861
30	79	158	237	396	1 188

TABLE IV: The total production of Zh_0 at the future muon collider in the context of the BLHM with $f = 1000$ GeV and $F = 6000$ GeV ($m_{Z'} = 5\,200$ GeV).

$f = 1000$ GeV, $F = 6000$ GeV					
\sqrt{s} TeV	$\mathcal{L} = 2\ ab^{-1}$	$\mathcal{L} = 4\ ab^{-1}$	$\mathcal{L} = 6\ ab^{-1}$	$\mathcal{L} = 10\ ab^{-1}$	$\mathcal{L} = 30\ ab^{-1}$
3	1 501	3 003	4 505	7 509	22 529
4	1 447	2 895	4 343	7 239	21 717
5	8 903	17 806	26 709	44 515	133 546
6	5 793	11 586	17 380	28 966	86 900
7	2 871	5 742	8 613	14 356	43 068
10	922	1 485	2 768	4 614	13 844
30	80	160	240	401	1 204

D. Heavy Higgs boson production H_0 in the BLHM

In this subsection, we present our results on the production cross-section of the Higgsstrahlung process $\mu^+\mu^- \rightarrow (Z, Z') \rightarrow ZH_0$, and analyze the impact of the parameters of the BLHM on this process. From Fig. 1, we can observe that the total cross-section of the production process $\mu^+\mu^- \rightarrow ZH_0$ receives contributions from the Z and Z' gauge bosons, and from the interference effects between them. In this manner, cross-sections $\sigma_Z(\mu^+\mu^- \rightarrow ZH_0)$, $\sigma_{Z'}(\mu^+\mu^- \rightarrow ZH_0)$ and $\sigma_{ZZ'}(\mu^+\mu^- \rightarrow ZH_0)$ contribute to the total cross-section $\sigma_T^{ZH_0}(\mu^+\mu^- \rightarrow ZH_0)$. These production cross-sections depend on the free parameters of the BLHM: f , F , and \sqrt{s} . Thus, in order to analyze the effects of \sqrt{s} on $\sigma_i(\mu^+\mu^- \rightarrow ZH_0)$ with $i = Z, Z', ZZ', T$, we generate the curves in Fig. 7 by setting the other input parameters to $f = 1000$ GeV and $F = 6000$ GeV. For these elections, the new heavy gauge boson Z' obtains a mass of about 5 200 GeV. In this figure, we observe that the curves associated to $\sigma_{Z'}$, $\sigma_{ZZ'}$, and $\sigma_T \equiv \sigma_T^{ZH_0}$ obtain large values around the resonance energy of the Z' boson, specifically, for the values of $\sqrt{s} \approx 5\,200, 5\,600, 5\,200$ GeV generate $\sigma_{Z'}(\mu^+\mu^- \rightarrow ZH_0) = 1.60 \times 10^{-3}$ fb, $\sigma_{ZZ'}(\mu^+\mu^- \rightarrow ZH_0) = 4.47 \times 10^{-4}$ fb and $\sigma_T(\mu^+\mu^- \rightarrow ZH_0) = 2.01 \times 10^{-3}$ fb, respectively. Regarding the cross-section $\sigma_Z(\mu^+\mu^- \rightarrow ZH_0)$, it reaches the maximum when $\sqrt{s} \approx 2\,000$ GeV, at this point

$$\sigma_Z(\mu^+\mu^- \rightarrow ZH_0) = 5.84 \times 10^{-4} \text{ fb.}$$

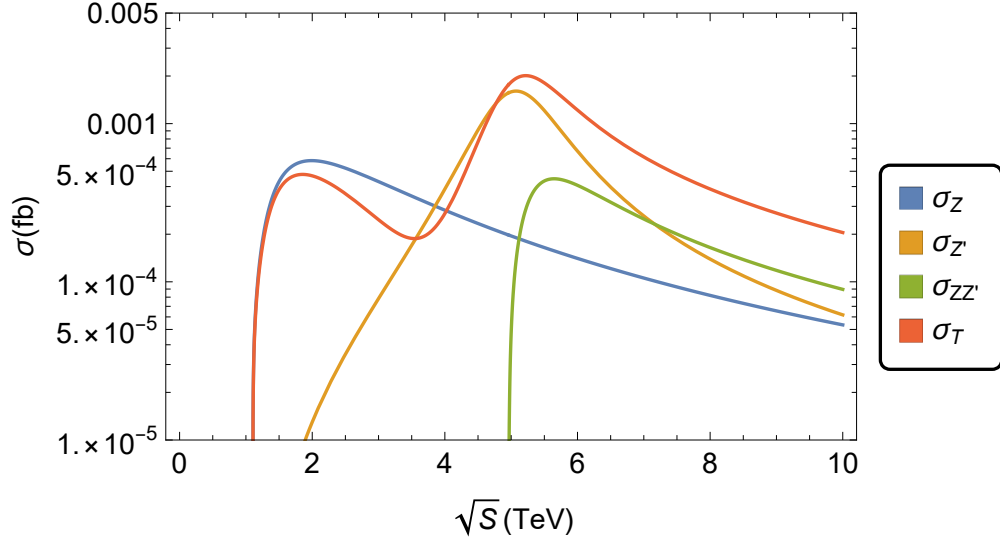


FIG. 7: The cross-section of the process $\mu^+\mu^- \rightarrow (Z, Z') \rightarrow ZH_0$ as a function of \sqrt{s} . The curves are generated for $f = 1000$ GeV and $F = 6000$ GeV (for $m_{Z'} = 5\ 200$ GeV), and correspond to σ_Z (Eq. (100)), $\sigma_{Z'}$ (Eq. (101)), $\sigma_{ZZ'}$ (Eq. (102)), and $\sigma_T \equiv \sigma_T^{ZH_0}$ (Eq. (99)).

In Fig. 8, we also present the production cross-section of the process $\mu^+\mu^- \rightarrow ZH_0$ as a function of \sqrt{s} while the energy scales, f and F , take on certain fixed values: $f = 1000$ GeV and $F = 4000$ GeV, $f = 1000$ GeV and $F = 5000$ GeV, and $f = 1000$ GeV and $F = 6000$ GeV. From this figure, a slight increase of the total cross-section $\sigma_T(\mu^+\mu^- \rightarrow ZH_0)$ is observed for small values of the F scale while for large values of the center-of-mass energy \sqrt{s} , $\sigma_T(\mu^+\mu^- \rightarrow ZH_0)$ becomes smaller. For the plotted curves, resonant effects dominate, i.e., the maximum peaks of each curve are reached just at the resonance of the Z' gauge boson: $\sigma_T(\sqrt{s}, 1000 \text{ GeV}, 4000 \text{ GeV}) = 3.93 \times 10^{-3} \text{ fb}$, $\sigma_T(\sqrt{s}, 1000 \text{ GeV}, 5000 \text{ GeV}) = 2.72 \times 10^{-3} \text{ fb}$, and $\sigma_T(\sqrt{s}, 1000 \text{ GeV}, 6000 \text{ GeV}) = 2.01 \times 10^{-3} \text{ fb}$ for the corresponding energies, $\sqrt{s} \approx 3\ 500, 4\ 300, 5\ 200$ GeV. In the BLHM scenario, the measure of the fine-tuning depends only on the f scale, as discussed above, for values of $f \in [1\ 000, 2\ 000]$ GeV, the absence of the fine-tuning prevails in the model, and for this reason, our plots have been generated for $f = 1\ 000$ GeV while allowing the other free parameters to vary.

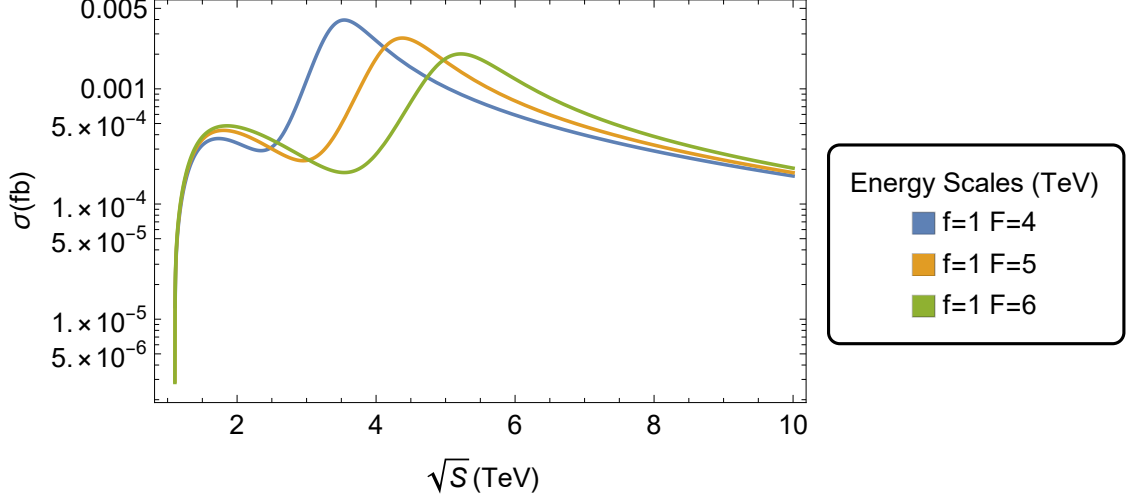


FIG. 8: The cross-section of the process $\mu^+\mu^- \rightarrow (Z, Z') \rightarrow ZH_0$ as a function of \sqrt{s} . The curves are generated for $f = 1000$ GeV and $F = 4000$ GeV, $f = 1000$ GeV and $F = 5000$ GeV, and $f = 1000$ GeV and $F = 6000$ GeV.

As part of our study, and as an indicator of the possible number of ZH_0 events to be produced in a future muon collider, we consider again the center-of-mass energies $\sqrt{s} = 3, 4, 5, 6, 7, 10, 30$ TeV and the integrated luminosities $\mathcal{L} = 2, 4, 6, 10, 30$ ab^{-1} [19, 43, 44]. In Tables V and VI we list the number of ZH_0 events arising when $f = 1000$ GeV and $F = 4000$ GeV, and $f = 1000$ GeV and $F = 6000$ GeV, respectively. According to our numerical data, the possibility of performing measurements for the Z' gauge boson and the heavy Higgs boson H_0 at the future high-energy muon collider is modest. For these cases of interest, resonant effects dominate over non-resonant effects. Thus, the total cross-section $\sigma_T(\mu^+\mu^- \rightarrow ZH_0)$ reaches its maximum value at the resonance of the heavy gauge boson Z' .

TABLE V: The total production of ZH_0 at the future muon collider in the context of the BLHM with $f = 1000$ GeV and $F = 4000$ GeV ($m_{Z'} = 3\,500$ GeV).

$f = 1000$ GeV, $F = 4000$ GeV					
\sqrt{s} TeV	$\mathcal{L} = 2\ ab^{-1}$	$\mathcal{L} = 4\ ab^{-1}$	$\mathcal{L} = 6\ ab^{-1}$	$\mathcal{L} = 10\ ab^{-1}$	$\mathcal{L} = 30\ ab^{-1}$
3	2	4	7	11	35
4	5	10	15	26	78
5	2	4	6	10	31
6	1	2	3	5	17
7	1	1	2	4	12
10	1	1	1	2	5
30	1	1	1	1	1

TABLE VI: The total production of ZH_0 at the future muon collider in the context of the BLHM with $f = 1000$ GeV and $F = 6000$ GeV ($m_{Z'} = 5\,200$ GeV).

$f = 1000$ GeV, $F = 6000$ GeV					
\sqrt{s} TeV	$\mathcal{L} = 2\ ab^{-1}$	$\mathcal{L} = 4\ ab^{-1}$	$\mathcal{L} = 6\ ab^{-1}$	$\mathcal{L} = 10\ ab^{-1}$	$\mathcal{L} = 30\ ab^{-1}$
3	1	1	1	2	7
4	1	1	1	2	8
5	3	7	10	18	54
6	2	4	7	12	36
7	1	2	3	6	18
10	1	1	2	2	6
30	1	1	1	1	1

VI. CONCLUSIONS

In this article, we have studied the Z' boson of the BLHM as a portal to signatures of Higgs bosons h_0 and H_0 through the Higgs-strahlung production processes $\mu^+\mu^- \rightarrow (Z, Z') \rightarrow Zh_0, ZH_0$, including both the resonant and non-resonant effects. The new Z'

boson is a hypothetical massive particle of spin 1 that is also predicted in other extensions of the SM and has been the subject of extensive phenomenological studies in recent years [45]. Experimentally, the Z' gauge boson will be searched at the LHC [34]. In the context of the BLHM, Higgs-strahlung productions $\mu^+\mu^- \rightarrow Zh_0, ZH_0$ are essential processes to study tree-level interactions: $Z'Zh_0, Z'ZH_0, ZZh_0$ and ZZH_0 . At the same time, the mentioned processes are helpful to test the consistency of the current parameter space of the BLHM.

As for the Higgs-strahlung process $\mu^+\mu^- \rightarrow Zh_0$, for its study we consider the BLHM contributions generated through the $Z'Zh_0$ and ZZh_0 couplings. We find that the relative correction of the total cross-section $\sigma_T(\mu^+\mu^- \rightarrow Zh_0)$ from its SM prediction can vary from 0 to 10%, which arises mainly from the modifications of the ZZh_0 coupling, and also from the contribution induced through the $Z'Zh_0$ interaction vertex. Our numerical data show that for reasonable values of the free parameters of the BLHM it can generate significant contributions to $\sigma_T(\mu^+\mu^- \rightarrow Zh_0)$. In most of the parameter space, the relative corrections' values are positive and decoupled at high scales from the \sqrt{s} parameter.

In the BLHM, we explore the phenomenological implications of the production cross-section of the processes $\mu^+\mu^- \rightarrow Zh_0, ZH_0$. As a result of our analysis, we find that the cross-sections $\sigma_T(\mu^+\mu^- \rightarrow Zh_0)$ and $\sigma_T(\mu^+\mu^- \rightarrow ZH_0)$ reach large values at the resonance of the heavy gauge boson Z' , when $\sqrt{s} = m_{Z'}$. $\sigma_T(\mu^+\mu^- \rightarrow Zh_0)$ and $\sigma_T(\mu^+\mu^- \rightarrow ZH_0)$ are also sensitive to variations in the F parameter, and the height of the resonance peaks for the Z' boson changes depending on the F scale values. Thus, the cross-sections $\sigma_T(\mu^+\mu^- \rightarrow Zh_0)$ and $\sigma_T(\mu^+\mu^- \rightarrow ZH_0)$ obtain large values when F obtains small values. Another input parameter involved in our cross-section calculations is the f scale, which is set to 1000 GeV to ensure the absence of fine-tuning in our phenomenological predictions.

To estimate the production of Higgs bosons h_0 and H_0 at the future muon collider, we use the energies and design luminosities of the muon collider with the center-of-mass energies of $\sqrt{s} = 3, 4, 5, 6, 7, 10, 30$ TeV and integrated luminosities of $\mathcal{L} = 2, 4, 6, 10, 30$ ab^{-1} [19, 43, 44]. We can observe from Tables III-VI that the total number of expected events for Zh_0 and ZH_0 at a future muon collider increase just at the resonance energy of the Z' boson. Our results show a very optimistic scenario for producing Higgs bosons h_0 and bosons Z in the future muon experiment. Regarding the production of Higgs bosons H_0 and bosons Z , these show a more conservative scenario.

Finally, studying the resonances is an excellent place to look for new physics. In this

regard, our results may be helpful to the scientific community and complement other studies performed in extended models. Our predictions presented in this work could be relevant for the community to prioritize future searches and experimental efforts.

Acknowledgements

J. M. Martínez-Martínez is a scholarship fellow of CONAHCyT. E. Cruz-Albaro appreciates the post-doctoral stay. A.G.R. and M.A.H.R. thank SNII and PROFEXCE (México).

Declarations

Data Availability Statement: All data generated or analyzed during this study are included in this article.

Appendix A: Feynman rules for the BLHM

In this Appendix, we provide the Feynman rules for the interaction vertices involved in the calculation of the Higgs-strahlung production processes $\mu^+\mu^- \rightarrow Zh_0, ZH_0$.

TABLE VII: Three-point couplings of one gauge boson to two leptons in the BLHM.

Particle	Couplings
$Z\bar{e}_i e_i$	$g_A^{Z\bar{e}_i e_i} = \frac{ig}{4c_W}$ $g_V^{Z\bar{e}_i e_i} = \frac{ig}{4c_W}(-1 + 4s_W^2)$
$Z'\bar{e}_i e_i$	$g_A^{Z'\bar{e}_i e_i} = \frac{igc_g}{8s_g} \left(2 + \frac{(c_g - s_g)s_g^2(c_g + s_g)(c_W^2 - 3s_W^2)v^2}{c_W^2(f^2 + F^2)} \right)$ $g_V^{Z'\bar{e}_i e_i} = -\frac{igc_g}{8s_g} \left(2 + \frac{(c_g - s_g)s_g^2(c_g + s_g)(c_W^2 + s_W^2)v^2}{c_W^2(f^2 + F^2)} \right)$

TABLE VIII: Three-point couplings of two gauge bosons to one Higgs boson in the BLHM.

Particle	Couplings
ZZh_0	$g_{ZZh_0} = \frac{gm_W \sin(\alpha + \beta)}{c_W^2} - \frac{s_W^2 v^3 (g^2 + g_Y^2)^2 \sin(\alpha + \beta)}{6g_Y^2 f^2}$ $- \frac{s_W v^3 x_s (g^2 + g_Y^2) \sin(\alpha + \beta) (-c_g^2 g g_Y + c_g s_g s_W (g^2 + g_Y^2) + g g_Y s_g^2)}{2c_g s_g g_Y^2 (f^2 + F^2)}$
$ZZ'h_0$	$g_{ZZ'h_0} = -\frac{gs_W v (c_g^2 - s_g^2) (g^2 + g_Y^2) \sin(\alpha + \beta)}{2c_g s_g g_Y} + \frac{gs_W v^3 (c_g^2 - s_g^2) (g^2 + g_Y^2) \sin(\alpha + \beta)}{6c_g s_g g_Y f^2}$ $+ \frac{v^3 x_s \sin(\alpha + \beta) (c_g^2 g g_Y s_W (g^2 + g_Y^2) + 2c_g s_g (g^4 s_W^2 + g^2 g_Y^2 (2s_W^2 + 1) + g_Y^4 s_W^2) - g g_Y s_g^2 s_W (g^2 + g_Y^2))}{2c_g s_g g_Y^2 (f^2 + F^2)}$
ZZH_0	$g_{ZZH_0} = \frac{s_W^2 v (g^2 + g_Y^2)^2 \cos(\alpha + \beta)}{2g_Y^2} - \frac{s_W^2 v^3 (g^2 + g_Y^2)^2 \cos(\alpha + \beta)}{6g_Y^2 f^2}$ $- \frac{s_W v^3 x_s (g^2 + g_Y^2) \cos(\alpha + \beta) (c_g^2 (-g) g_Y + c_g s_g s_W (g^2 + g_Y^2) + g g_Y s_g^2)}{2c_g s_g g_Y^2 (f^2 + F^2)}$
$ZZ'H_0$	$g_{ZZ'H_0} = -\frac{gs_W v (c_g^2 - s_g^2) (g^2 + g_Y^2) \cos(\alpha + \beta)}{2c_g s_g g_Y} + \frac{gs_W v^3 (c_g^2 - s_g^2) (g^2 + g_Y^2) \cos(\alpha + \beta)}{6c_g s_g g_Y f^2}$ $+ \frac{v^3 x_s \cos(\alpha + \beta) (c_g^2 g g_Y s_W (g^2 + g_Y^2) + 2c_g s_g (g^4 s_W^2 + g^2 g_Y^2 (2s_W^2 + 1) + g_Y^4 s_W^2) - g g_Y s_g^2 s_W (g^2 + g_Y^2))}{2c_g s_g g_Y^2 (f^2 + F^2)}$

-
- [1] G. Aad *et al.* (ATLAS Collaboration), *Phys. Lett. B* **716**, 1 (2012).
- [2] S. Chatrchyan *et al.* (CMS Collaboration), *Phys. Lett. B* **716**, 30 (2012).
- [3] G. Aad *et al.* (ATLAS Collaboration), *Eur. Phys. J. C* **75**, 476 (2015).
- [4] V. Khachatryan *et al.* (CMS Collaboration), *Phys. Rev. D* **92**, 012004 (2015).
- [5] G. Aad *et al.* (ATLAS Collaboration), *Eur. Phys. J. C* **76**, 6 (2016).
- [6] V. Khachatryan *et al.* (CMS Collaboration), *Eur. Phys. J. C* **75**, 212 (2015).
- [7] G. Aad *et al.* (ATLAS and CMS Collaborations), *JHEP* **08**, 045 (2016).
- [8] N. Arkani-Hamed, A. G. Cohen, E. Katz and A. E. Nelson, *JHEP* **07**, 034 (2002).
- [9] S. Chang, *JHEP* **12**, 057 (2003).
- [10] T. Han, H. E. Logan, B. McElrath and L. T. Wang, *Phys. Rev. D* **67**, 095004 (2003).
- [11] S. Chang and J. G. Wacker, *Phys. Rev. D* **69**, 035002 (2004).
- [12] M. Schmaltz, *JHEP* **08**, 056 (2004).
- [13] M. Schmaltz, D. Stolarski and J. Thaler, *JHEP* **09**, 018 (2010).
- [14] C. Csaki, J. Hubisz, G. D. Kribs, P. Meade and J. Terning, *Phys. Rev. D* **67**, 115002 (2003).
- [15] C. Csaki, J. Hubisz, G. D. Kribs, P. Meade and J. Terning, *Phys. Rev. D* **68**, 035009 (2003).
- [16] J. A. Casas, J. R. Espinosa and I. Hidalgo, *JHEP* **03**, 038 (2005).
- [17] P. Kalyniak, T. Martin and K. Moats, *Phys. Rev. D* **91**, 013010 (2015).
- [18] S. Godfrey, T. Gregoire, P. Kalyniak, T. A. W. Martin and K. Moats, *JHEP* **04**, 032 (2012).
- [19] D. Stratakis *et al.* (Muon Collider Collaboration), *A Muon Collider Facility for Physics Discovery*, arXiv:2203.08033 [physics.acc-ph].
- [20] C. Accettura, D. Adams, R. Agarwal, C. Ahdida, C. Aimè, N. Amapane, D. Amorim, P. Andreetto, F. Anulli and R. Appleby, *et al.*, *Eur. Phys. J. C* **83**, 864 (2023); Erratum: *Eur. Phys. J. C* **84**, 36 (2024).
- [21] T. Cisneros-Pérez, M. A. Hernández-Ruíz, A. Gutiérrez-Rodríguez and E. Cruz-Albaro, *Eur. Phys. J. C* **83**, 1093 (2023).
- [22] E. Cruz-Albaro, A. Gutierrez-Rodriguez, M. A. Hernandez-Ruiz and T. Cisneros-Perez, *Eur. Phys. J. Plus* **138**, 506 (2023).
- [23] E. Cruz-Albaro, A. Gutiérrez-Rodríguez, J. I. Aranda and F. Ramírez-Zavaleta, *Eur. Phys. J. C* **82**, 1095 (2022).

- [24] E. Cruz-Albaro and A. Gutiérrez-Rodríguez, *Eur. Phys. J. Plus* **137**, 1295 (2022).
- [25] E. Cruz-Albaro, A. Gutiérrez-Rodríguez, D. Espinosa-Gómez, T. Cisneros-Pérez and F. Ramírez-Zavaleta, arXiv:2403.08225 [hep-ph]. Accepted for publication in the Physical Review D (2024).
- [26] T. Cisneros-Pérez, E. Cruz-Albaro, A. Y. Ojeda-Castañeda and S. E. Solís-Núñez, arXiv:2404.00483 [hep-ph].
- [27] T. Cisneros-Pérez, M. A. Hernández-Ruíz, A. Ramirez-Morales, A. Gutiérrez-Rodríguez and J. Montaña-Domínguez, arXiv:2403.08021 [hep-ph].
- [28] M. Schmaltz and J. Thaler, *JHEP* **03**, 137 (2009).
- [29] K. P. Moats, *Phenomenology of Little Higgs models at the Large Hadron Collider*, 2012. doi:10.22215/etd/2012-09748.
- [30] D. Eriksson, J. Rathsman and O. Stal, *Comput. Phys. Commun.* **181**, 189 (2010).
- [31] T. A. W. Martin, *Examining extra neutral gauge bosons in non-universal models and exploring the phenomenology of the Bestest Little Higgs model at the LHC*, 2012. doi:10.22215/etd/2012-09697.
- [32] S. P. Martin, *Adv. Ser. Direct. High Energy Phys.* **18**, 1 (1998).
- [33] A. Gutiérrez-Rodríguez, E. Cruz-Albaro and D. Espinosa-Gómez, arXiv:2312.08560 [hep-ph].
- [34] R. L. Workman *et al.* (Particle Data Group), *Prog. Theor. Exp. Phys.* **2022**, 083C01 (2022).
- [35] J. Ellis, M. K. Gaillard, and D. V. Nanopoulos, *Nucl. Phys.* **B106**, 292 (1976).
- [36] B. L. Ioffe and V. A. Khoze, *Sov. J. Part. Nucl.* **9**, 50 (1978).
- [37] B. W. Lee, C. Quigg, and H. B. Thacker, *Phys. Rev.* **D16**, 1519 (1977).
- [38] J. D. Bjorken, Proceeding *Summer Institute on Particle Physics*, SLAC Report 198 (1976).
- [39] V. D. Barger, *et al.*, *Phys. Rev.* **D49**, 79 (1994).
- [40] W. Altmannshofer and D. M. Straub, *JHEP* **09**, 078 (2010).
- [41] G. Aad, *et al.* (ATLAS Collaboration), *Eur. Phys. J.* **C81**, 396 (2021).
- [42] A. M. Sirunyan *et al.* (CMS Collaboration), *JHEP* **03**, 055 (2020).
- [43] J. de Blas *et al.* (Muon Collider Collaboration), arXiv:2203.07261 [hep-ph].
- [44] H. Al Ali, N. Arkani-Hamed, I. Banta, S. Benevedes, D. Buttazzo, T. Cai, J. Cheng, T. Cohen, N. Craig and M. Ekhterachian, *et al.*, *Rept. Prog. Phys.* **85**, 084201 (2022).
- [45] A. Leike, *Phys. Rept.* **317**, 143 (1999).